Final Report

A three-dimensional organoid model recapitulates tumorigenic aspects and drug responses of vitreous seeds in human retinoblastoma

Dr. Rossukon Kaewkhaw

July/ 2018

Contract No. MRG 5980031

Final Report

A three-dimensional organoid model recapitulates tumorigenic aspects and drug responses of vitreous seeds in human retinoblastoma

Dr. Rossukon Kaewkhaw
Section for Translational Medicine, Faculty of Medicine Ramathibodi Hospital
Mahidol University

Project Granted by the Thailand Research Fund

Abstract

Project Code : MRG 5980031

Project Title : A three-dimensional organoid model recapitulates tumorigenic aspects and drug responses of vitreous seeds in human retinoblastoma

Investigator : Dr. Rossukon Kaewkhaw

E-mail Address : ross.kaewkhaw@gmail.com

Project Period : 2 years

Abstract:

Persistent or recurrent vitreous seeds in advanced retinoblastoma are a major cause of therapeutic failure as a result of drug resistance. This necessitates the development of novel therapies and thus requires a model of vitreous seeds for testing candidate therapeutics. To this aim, we established and characterized a three-dimensional, self-organizing tumor organoid model derived from chemotherapy-naïve primary tumor tissue. The responses of tumor organoids to drugs with final clinical doses achieved in vitreous were determined and compared to relate organoid model to the seeds, in terms of drug sensitivities. We found that tumor organoids preserved histogenesis, DNA copy-number alterations, as well as gene and protein expression of the parental tissue. Cone signal circuitry (M/L+ cells) and glial tumor microenvironment (GFAP+ cells) were primarily present in organoids. Topotecan alone or the combined drug regimen of topotecan and melphalan effectively targeted proliferative tumor cones (RXRγ+ Ki67+) in organoids after 24 h exposure to drugs, blocking mitotic entry. In contrast, methotrexate showed the least efficacy against tumor cells. The results suggest that the responses of organoids were consistent with those of vitreous seeds. Patient-derived tumor organoids enable the creation of a faithful model to use in examining novel therapeutics for vitreous seed control.

Keywords : organoid; retinoblastoma; vitreous seed; cancer model; anticancer drugs

บทคัดย่อ

มะเร็งจอประสาทตาขั้นรุกลามเข้าไปในวุ้นตา ส่วนใหญ่ไม่ตอบสนองต่อยาเคมีบำบัด ส่งผลให้การรักษาไม่ประสบผลสำเร็จ ทำให้ต้องมีการพัฒนายาเพื่อการรักษาที่มีประสิทธิภาพ การใช้โมเดลที่สามารถจำลองเนื้อเยื่อมะเร็งจอประสาทตาชนิดรุกลาม มีความสำคัญในการทดสอบตัวยา และการแปลผลที่ถูกต้อง ดั้งนั้น จุดประสงค์ของงานวิจัยนี้คือ สร้างและทดสอบคุณลักษณะของโมเดลมะเร็งจอประสาทตาชนิดรุกลามเข้าไปในวุ้นตา โดยใช้เทคนิคออร์แกนอยด์สร้างเนื้อเยื่อมะเร็งในหลอดทดลองจากเนื้อเยื่อมะเร็งของผู้ป่วยที่ไม่เคยถูกให้สารเคมีบำบัด เพื่อทดสอบการตอบสนองต่อยาต้านมะเร็งชนิดต่างๆ สารละลายเคมีบำบัดถูกผสมเข้ากับอาหารในระบบเลี้ยงออร์แกนอยด์ โดยที่สารเคมีบำบัดถูกเตรียมให้มีความเข้มข้นสุดท้ายเท่ากับความเข้มข้นของยาในลูกตาของผู้ป่วย โมเดลออร์แกนอยด์และมะเร็งจอประสาทตาขั้นรุกลามยังถูกเชื่อมโยงในแง่ของการตอบสนองต่อสารเคมีบำบัดชนิดเดียวกัน ผลการทดลองแสดงให้เห็นว่า ลักษณะทางเนื้อเยื่อ, ความผิดปกติของจำนวนชุดดีเอ็นเอ และการแสดงออกของยีนรวมถึงการผลิตโปรตีนของโมเดลออร์แกนอยด์เหมือนกับเนื้อเยื่อมะเร็งที่ถูกใช้สร้างออร์แกนอยด์ เรายังพบว่าออร์แกนอยด์ประกอบไปด้วยเซลล์มะเร็งที่มีคุณสมบัติของเซลล์ประสาทรับแสงชนิดโคน และเซลล์เกลีย ผลการทดสอบสารเคมีบำบัดแสดงให้เห็นว่าการใช้ topotecan อย่างเดียว หรือใช้ร่วมกับ melphalan สามารถฆ่าเซลล์มะเร็งได้อย่างมีประสิทธิภาพ ป้องกันการแบ่งตัวของเซลล์มะเร็งหลังจากถูกสารเคมีบำบัดนาน 24 ชม. เรายังพบว่า methotrexate มีฤทธิ์การต้านมะเร็งน้อยที่สุด ผลการทดลองชี้ให้เห็นว่าการตอบสนองต่อสารเคมีบำบัดของออร์แกนอยด์เหมือนกับการตอบสนองต่อสารเคมีบำบัดชนิดเดียวกันของมะเร็งจอประสาทตาขั้นรุกลามเข้าไปในวุ้นตา ดังนั้นออร์แกนอยด์จากเนื้อเยื่อมะเร็งของผู้ป่วยเหมาะสมต่อการใช้เป็นโมเดลเพื่อทดสอบหายาตัวใหม่สำหรับการรักษามะเร็งจอประสาทตาขั้นรุกลามเข้าไปในวุ้นตา

คำสำคัญ: ออร์แกนอยด์; มะเร็งจอประสาทตา; มะเร็งจอประสาทตาขั้นรุกลามเข้าไปในวุ้นตา; โมเดลมะเร็ง; ยาต้านมะเร็ง

Final report content:

1. Abstract

Persistent or recurrent vitreous seeds in advanced retinoblastoma are a major cause of therapeutic failure as a result of drug resistance. This necessitates the development of novel therapies and thus requires a model of vitreous seeds for testing candidate therapeutics. To this aim, we established and characterized a three-dimensional, self-organizing tumor organoid model derived from chemotherapy-naïve primary tumor tissue. The responses of tumor organoids to drugs with final clinical doses achieved in vitreous were determined and compared to relate organoid model to the seeds, in terms of drug sensitivities. We found that tumor organoids preserved histogenesis, DNA copy-number alterations, as well as gene and protein expression of the parental tissue. Cone signal circuitry (M/L+ cells) and glial tumor microenvironment (GFAP+ cells) were primarily present in organoids. Topotecan alone or the combined drug regimen of topotecan and melphalan effectively targeted proliferative tumor cones (RXRγ+ Ki67+) in organoids after 24 h exposure to drugs, blocking mitotic entry. In contrast, methotrexate showed the least efficacy against tumor cells. The results suggest that the responses of organoids were consistent with those of vitreous seeds. Patient-derived tumor organoids enable the creation of a faithful model to use in examining novel therapeutics for vitreous seed control.

2. Executive summary (including; Introduction to Research, Literature review, Objective, Research methodology)

We have reported unexpected problems and accordingly, experimental plans were changed to meet objectives (explained in 18-month report). This report shows successful development of a preclinical model of vitreous seeds in retinoblastoma, known as retinoblastoma organoids. As a proof-of-concept of vitreous seed model, we determine and compare the responses of tumor organoids to clinically used drugs for intravitreal chemotherapy (melphalan, topotecan, and methotrexate) to relate organoid model to the seeds, in term of drug sensitivities. Our data suggest that tumor organoids are faithful preclinical model for examining novel therapeutics for vitreous seed control. We hence include Introduction to Research, Literature review, Objective, Research methodology for this report as follows.

Retinoblastoma (RB) is a serious childhood retinal tumor that, if left untreated, can cause death within 1–2 years. Current management of RB aims to salvage both the globe and visual function, in addition to saving the patient's life. However, persistent or recurrent vitreous seeds in advanced intraocular RB are a major cause of RB therapeutic failure, representing the primary limitation for globe salvage[1]. Systemic intravenous chemotherapy encounters difficulty in controlling vitreous seeds that exhibit massive and diffuse infiltration, finally leading to enucleation[1]. The minimal response to chemotherapy is partly because of non-vascularization in the vitreous, causing reduced concentration of delivered drugs in the vitreous.

In additional to primary treatment intravitreal chemotherapy is locally applied to increase drug accessibility and shows impressive control of seeds with minimal complications[2, 3]. Melphalan is extensively used despite its high toxicity[2, 3]; this therapy results in an overall globe salvage rate of 68%[1]. A few drugs, such as topotecan and methotrexate, have been used with variable degrees of success[4, 5]; the combination of topotecan and melphalan is optional for refractory and recurrent vitreous seeds[6]. However, case reports have shown failure in some patients, leading to enucleation[1-5]. This highlights the need for drug development and evaluation to ascertain efficacy and safety. Representative and robust models of vitreous seeds are thus required to determine the activities of candidate therapeutic agents for seed control.

Genetically engineered mouse models (GEMMs) are powerful tools to study pathogenesis and develop new therapies for RB[7, 8]. Unlike in human RB, additional genes must be inactivated together with Rb1 to induce tumorigenesis in mice[8-10]. Molecular and cellular analyses indicate that mouse RB has properties of amacrine/horizontal interneurons, reflective of the tumor cells of origin[7, 10, 11]. In contrast, cones are frequently identified in human RB[12] and significantly sensitive to cancerous transformation when the RB1 gene is lost in the human retina[13]. Furthermore, the epigenetic landscape significantly differs between mouse and human RB[11, 14]. Some candidates for molecular targeted therapy, such as epigenetically deregulated SYK[15] in human RB, appear to be normally regulated in GEMMs[14]. This indicates that different mechanisms underlying tumorigenesis exist between humans and mice.

Advances in organoid technology allow the generation of three-dimensional (3-D), self-organizing tissue that encompasses multiple lineages through a nature-mimicking

process. Accordingly, human and murine organoids have been generated from pluripotent or tissue stem cells in both healthy and diseased conditions[16] and then used to facilitate better understanding in biology and pathology[17-20]. Solid tumor tissues from patients have been used to generate organoids that retain molecular and histopathologic features of the original primary tumor tissue. This has been demonstrated in colon[21, 22], breast[23], liver[24], prostate[25], and pancreatic tumors[26], but has not yet been demonstrated for retinal tumors. Here, we aim to establish model of vitreous seeds through organoid culture derived from enucleated RB tissues for drug testing. Cellular and molecular features are thoroughly characterized to ascertain the presentation of tumorigenic aspects of the parental tumors in organoids after short and long-term culture. As a proof-of-concept of vitreous seed model, we determine and compare the responses of tumor organoids to clinically used drugs for intravitreal chemotherapy[1-6] to relate organoid model to the seeds, in term of drug sensitivities. We further demonstrate that drugs with greater efficacy not only induce cell death, but also preferentially target proliferative tumor cones, rather than resting cones. Thus, organoids provide opportunities for drug testing and the development of targeted therapies for vitreous seed control in advanced RB.

Materials and Methods

Human tissues

RB tissues (stage E, according to the International Classification for Intraocular RB) were collected directly from patients undergoing enucleation. Tumor tissue samples after incision were used for organoid culture and for analyses of DNA copy number alterations and gene expression profiles. Blood was drawn from patients for analysis of DNA copy number. All experimental protocols were approved by IRB at Faculty of Medicine, Ramathibodi Hospital, Mahidol University (protocol number ID11-58-53 and ID07-60-14). All methods were performed in accordance with the relevant guidelines and regulations. Informed consent was obtained from a parent of patients before collecting the samples.

RB organoid culture

Primary RB samples were collected in ice-cold Dulbecco's Modified Eagle Medium: Nutrient Mixture F-12 (DMEM/F-12) containing antibiotics. Tumor tissues were finely minced and incubated in ACCUMAX™ (Chemicon) for 30 min at 37°C. One volume of PBS was added to the cell solution, which was then centrifuged at 300 □ g for 5 min.

Supernatant was removed and cell pellets were resuspended in cold organoid medium (Neurobasal medium (Invitrogen) supplemented with 20 ng/mL epidermal growth factor (EGF; R&D Systems), 10 ng/mL basic fibroblast growth factor (bFGF; Peprotech), 1X B27 (Invitrogen), 2.5% knockout serum replacement (KSR), 2.5% fetal bovine serum (FBS), 20 mM Glutamax, 1 mM sodium pyruvate, 0.25 µg/mL amphotericin B, and 100 U/mL penicillin-streptomycin. Tumor cell solution was embedded in Matrigel® (growth factor reduced, Corning) at a 1:1.8 ratio of cell solution to Matrigel® solution. A total of 20 µL mixed cell-gel solution was added to six-well plates via 5-7 drops/well and solidified in an incubator (37°C) for 30–45 min. Organoid medium was added to cover the gel drops and cultures were maintained in a humidified incubator, with 5% CO2, at 37°C. RB organoids were manually dissociated and passaged at a 1:3 or 1:4 ratio every 3–4 weeks by embedding in fresh Matrigel®. Cold freezing medium (organoid medium containing 10% dimethylsulfoxide) was used to freeze organoids at -80°C for 24 h prior to long-term storage in liquid nitrogen.

Drug treatments

Drugs (pharmaceutical grade) were further diluted with 0.9% NaCl to obtain concentrations equivalent to the final clinical dose achieved in the vitreous, including melphalan at 8 (10), 16 (20) and 32 (40) µM (µg of delivered drugs in vitreous-containing 4 mL fluid), methotrexate at 275 µM (400 µg), and a combination of melphalan at 16 µM (20 µg) and topotecan at 11 µM (30 µg). Organoids (< passage 5) were incubated with drugs for 24 or 72 h. NaCl (0.02% final concentration in culture) was used as a control.

Histology, immunofluorescence and imaging, cell cycle, copy number, and gene expression analyses are described in the Supplementary Information.

Data Availability

All data generated or analyzed during this study are included in this published article and its Supplementary Information files (Appendix)

3. Results

Establishment of expansible RB organoids

Fresh surgical specimens of chemotherapy-naïve RB were obtained and processed for organoid derivation (∼0.3 cm3 tissue), as well as genomic and transcriptomic analyses. Tissue was mechanically and enzymatically dissociated; dissociated cells were mixed in

Matrigel® solution and plated as adherent Matrigel® drops which were overlaid with culture medium. We initially attempted to grow tumor organoids in medium (insulin, transferrin, N2, and FBS) for retinal organoids derived from pluripotent stem cells[19], which failed to support the growth. We then used mitogens (EGF and FGF2, known to support the survival of retinal cells[27]), serum replacement, and culture medium supporting the growth of neural progenitors. This newly formulated medium supported the proliferation of patient-derived cells that previously failed to grow (data not shown). Hence, we used newly formulated medium, in combination with Matrigel®, to establish tumor organoid cultures from the RB tissues of a new patient. This method efficiently allowed generation of tumor organoids and long-term expansion (>8 passages). A cluster of cells initially formed in Matrigel®, then enlarged and became dense and solid (Fig. 1a–c). Organoids were present in multiple sizes up to 1 mm in each single drop of Matrigel® at 3 weeks post-seeding; the cultures could be serially expanded with a consistent passaging ratio of 1:3–1:4 (Fig. 1a and 1b). Individual organoids displayed dense cellular organization of elements resembling rosette formation (Fig. 1c–f). In addition, RB organoids could be stored and resurrected from long-term storage in liquid nitrogen (up to 5 months' storage was tested) and retained normal cellular structure (data not shown).

RB organoids maintain cellular features of parental tumor

Histological analysis revealed that patient-derived RB tissue filled almost the entire globe and displayed massive choroidal and laminar optic nerve invasion (Fig. 2a–c). The parental RB demonstrated cuboidal cells with hyperchromatic nuclei and scant cytoplasm; this morphology was also found in tumor organoids (Fig. 2d–g). Tumor cells in a circular arrangement, with polarization of the cytoplasm toward the central lumen, indicated the formation of Flexner-Wintersteiner rosettes in organoids, resembling parental tumor tissue (Fig. 2f–g). The presence of Homer-Wright rosettes with neuropil in the lumen, as in primary tumors, was also identified in tumor organoids (Fig. 2f–g). In addition, mitotic figures were frequently present while apoptotic cells were distributed in an irregular fashion among viable cells in primary tumor tissue (Fig. S1a). This was consistent with features of tumor organoids, in which Ki67+ cells were widely distributed among dividing cells at the rim of organoids (Fig. S1b–e). CC3+ cells indicated that apoptosis occurred sporadically in organoids (Fig. S1f, g).

To determine cellular phenotypes, retinal cell and Ki67-proliferative markers were co-labeled in tumor organoids and the corresponding patient-derived tissue (Fig. 2h–o). This co-labeling enabled identification of a specific type of retinal tumor cell, which had the capability of neoplastic growth. Immunostaining revealed that retinoid X receptor-γ (RXRγ) and thyroid hormone receptor β2 (TRβ2), transcription factors important for the differentiation and maintenance of M/L cone identity28, 29, were detected in a majority of tumor cells within tissues and organoids (Fig. 2h–k). A subset of RXRγ+ and TRβ2+ cells was co-labeled with Ki67 (Fig. 2h–k). Detection of M/L opsin+ cells and M/L opsin+ Ki67+ cells confirmed the presence of neoplastic M/L cones in primary tissue and organoids (Fig. 2l, m). In contrast, S opsin+ cells were rarely detected and did not express Ki67 (Fig. S2a, b), suggesting that S opsin+ cells are non-proliferative. The expression of rod cell markers (neural retina-specific leucine zipper protein (NRL) and rhodopsin) was not detected in organoids and parental tumor tissue (Fig. S2c–f). In addition to photoreceptors, we examined organoids and their corresponding RB tissue for the expression of other retinal cell markers (Fig. S2g–p). Glial fibrillary acidic protein (GFAP)+ Ki67- cells were detected, suggesting the presence of non-proliferative glial cells in tumor organoids, similar to parental tumor tissue (Fig. 2n, o). In contrast, retinal progenitor (CHX10 and PAX6), ganglion (BRN3 and PAX6), bipolar (CHX10), amacrine (PROX1, AP2-α, and PAX6), and horizontal (PROX1 and PAX6) cells were absent, a finding that concurred with data from tumor tissue (Fig. S2g–p). Altogether, the results demonstrated that RB organoids recapitulated and retained the histological characteristics and retinal protein expression of the parental tumor tissue. Detailed analysis also indicated that neoplastic cells retained M/L cone phenotypes, even after long-term expansion in culture or storage in liquid nitrogen, in the same culture conditions (data not shown).

RB organoids retain genetic alterations of original tumor tissue

While the initiation of RB occurs as a result of RB1 biallelic loss, recurrent genomic gains and losses drive tumor progression. These alterations were determined in organoid cultures at 6 (P1), 13 (P2), and 19 (P5) weeks, in comparisons of tumor tissue matched with peripheral blood. Screening for RB1 mutations identified a large deletion (13q13.1–13q22.2) spanning the RB1 gene (Fig. 3a) as a germline mutation. An additional mutation (g.41924A>G) in retinal cells that became cancerous transformation resulted in defective splicing of RB1 transcripts. The biallelic loss of RB1 was present in

patient-derived organoids (Fig. 3a). The recurrent regional gains (>3 Mb) were consistently identified at 6p25.3–6p21.1 and 19p12–p11; losses occurred at 10q25.2–10q26.3 in parental tumor and organoids at different serial passages (Fig. 3a). In addition, recurrent copy number aberrations were frequently found in tumor organoid cells, indicating that sub-clonal populations found in tumor tissue were enriched in organoids; this was consistently maintained with serial passaging (Fig. 3 and S3a, b).

Two additional large regional gains (2p25.3–2p12 and 12q23.3–12q24.33) were identified in organoids (Fig. 3a and S3c, d); sub-clonal populations with these gains were further enriched with serial passaging (Fig. S3c, d). In addition, focal lesions (<3 Mb) were detected within the same fragments, with large regional gains consistently identified at chromosomes 2 and 6 and inconsistently identified at chromosome 16 (Fig. 3b). Somatic copy number alterations, including 1q, 2p, and 6p gains, as well as 16q loss, are commonly identified in RB[30, 31]. In addition, the recurrent 6p gain is associated with 2p gain, while the 1q gain is associated with 16q loss; the former association precedes the latter and thus is identified in RB tumors from patients diagnosed at younger age[32]. This suggests that 2p gain could be expected in organoid cells that were derived from the tumor with the recurrent 6p gain in our young patient at 7 months of age at diagnosis. Loss of heterozygosity was consistently maintained between tissue and organoids at different passages (data not shown).

Gene expression profile reflects the origin of RB in tumor organoids

Gene expression profiling from RNA-seq data was conducted to determine whether tumor organoids retain a gene signature of the parental tumor, reflecting the histogenesis of RB. Since the tumor was diagnosed at early age (7 months) in our RB patient, we included published transcriptome data of fetal retina (19 weeks)[18] and RB[11] for analysis (Fig. 4, S4, S5). Gene profiling analysis revealed that tumor organoids strongly correlated with the parental tumor tissue and were consistent between passages (Fig. 4a). As expected, the gene signatures indicated that the organoids and tumor tissue had a higher degree of correlation with primary RB than with normal developing retina (Fig. 4a). Furthermore, gene expression profiles of our samples were more readily distinguishable from normal retina (Fig. 4a) than in reported cases of RB, suggesting a higher purity of tumor cellularity in our samples. Transcriptomes of retina-enriched genes demonstrated that tumor organoids and the patient's tumor had high expression levels of cone-enriched genes (Fig. S4a), consistent with the analysis of protein expression. In addition, cone-associated genes that are susceptible to RB

transformation were upregulated in tumor tissue and organoids, in response to RB1 inactivation (Fig. S4b).

Functional annotation of differentially expressed genes between tumor organoids and fetal retina revealed that enrichment for the gene ontology (GO) associated with sensory perception was the most significant (Fig. 4b, S5a). We found that downregulated genes in organoids and tumor tissue, compared with fetal retina, were associated with the development and function of retinal neurons [ganglion (POU4F1 (BRN3A), KCNA2, and SCN1A), horizontal and amacrine (TFAP2A (AP2-α) and PAX6), and bipolar (VSX1 and GRM6) cells], Müller glial (RLBP1 and SCL1A3) and retinal progenitor (VSX2 and PAX6) cells (Fig. 4b). In addition, rod-enriched genes, including NRL, NR2E3, CNGA1, and PDE6G, were downregulated in tumor, but highly expressed in normal retina, where rods outnumber cones (Fig. 4b). In contrast, cone-enriched genes (PDE6C and ARR3) were upregulated in tumor tissue and further enriched in tumor organoids (Fig. 4b).

Furthermore, cell fate commitment was enriched as the second most significant GO (Fig. 4c, S5a). Concomitantly, we found that cell fate regulatory genes in retinal neuronal lineages were downregulated in tumor organoids and tissue, compared with fetal retina. These included early expressed genes in retinal development (TBX3, PAX6, NR2E1, EYA1, and GLI3) and regulatory genes for maintaining the retinal progenitor program (Notch signaling: HES5 and HEY2). Similarly, downregulation was detected for genes directing neurogenesis (ASCL1 and MYT1) and the formation of more specific retinal cell types [horizontal and amacrine (PROX1), ganglion (ISL1, POU4F1, and POU6F2) and rod (MEF2C) cells] (Fig.4c). However, we found that a set of regulatory genes governing mesodermal cell lineage was up-regulated in tumor organoids and tissue, compared with normal retina (Fig. 4c). These genes were normally expressed in developing mesoderm (TBX6, WNT11, PITX1, FEV and CYP26B1). Likewise, a set of genes functioning in the specification of mesodermal cells (MESP1, TBX1, NKX2.5, SIX1, SIX2, GATA2, and MYOD1) was enriched in organoids and tissue (Fig. 4c). Altogether, this suggested that tumor organoids contained hybrid gene signatures for both cone and mesodermal cells. Furthermore, tumor invasion-associated genes (MMP17 and ITGA3) were upregulated in tumor organoids and tissue (Fig. S5a, b). A similar phenomenon was observed for the expression level of SYK, contributing to tumor progression after RB1 inactivation15 (Fig. S5a, c). A set of genes (MIF, THBH4, TGFB1, DDT, NR4A1, and PRKCD) implicated in the proliferation and invasion of tumor

cells was upregulated, whereas genes (SEMA3A, PLEXNA4, EPHA5, and NGFR) functioning in normal axonal growth and guidance were downregulated in our samples (Fig. S5c). This was indicative of the invasive and metastatic capacities of tumor organoids, consistent with the metastatic characteristics of the primary tumor (Fig. 2a–c).

RB organoids allow in vitro evaluation of the clinical activity of anticancer drugs for vitreous seed control

To determine whether drug responses of vitreous seeds are reproduced in organoids tumor organoids were treated with clinically used drugs for intravitreal chemotherapy (melphalan, topotecan, and methotrexate). Furthermore, comparisons were made between combined drug (melphalan and topotecan) and single drug regimens, which are challenging to systematically perform in clinics. Concentrations of drugs used in this study were equivalent to the final clinical dose achieved in the vitreous. Since tumor organoids exhibited cellular structure similar to tumor tissue (Fig. 1d–f), we demonstrated that drug accessibility and uptake occurred in the deepest area at the core of tumor organoids, indicated by elevated γ-H2AX foci, a DNA damage response marker (Fig. S6).

Cell cycle profiles (Fig. 5a, b) and apoptosis (Fig.5c–j) were determined in response to anticancer drugs for short (24 h) and long (72 h) exposure times. Melphalan, a common clinical therapy for vitreous seed control, was examined at different doses. Melphalan at 8 μM significantly reduced the number of G0/G1-phase cells ($p < 0.0001$) and induced S-phase arrest ($p < 0.0001$) (Fig. 5a, b). However, this concentration was not sufficient to cause significant cell death, as there was no alteration in the number of sub-G1 and CC3+ cells in treated organoids (Fig. 5a-d, j). Higher concentrations of melphalan (16 and 32 μM) significantly induced elevated sub-G1 fractions (vs. vehicle, $p = 0.0048$ and $p < 0.0001$) (Fig.5a, b), consistent with CC3+ staining for 32 μM melphalan (vs. vehicle, $p < 0.001$) (Fig. 5c, e, f, j). Elevated sub-G1 correlated with reduction of G0/G1 fractions (vs. vehicle, $p < 0.0001$) for both 16 and 32 μM concentrations of melphalan. The effect was more deleterious for the highest dose, reducing the G2/M-phase fraction (vs. vehicle, $p = 0.0277$) (Fig. 5a, b).

Unlike 8 and 16 μM melphalan, tumor organoid cells treated with 32 μM melphalan did not arrest in S phase, but underwent apoptosis in sub-G1 phase (8 vs. 32 μM, $p <$

0.0001; 16 vs. 32 μM, p = 0.0103) (Fig. 5a, b), consistent with CC3+ staining (8 vs. 32 μM, p = 0.0001; 16 vs. 32 μM, p = 0.0057) (Fig. 5j). This suggested that after 24 h of exposure, 8 and 16 μM melphalan preferentially induced S-phase arrest; in contrast, 32 μM melphalan immediately targeted tumor organoid cells. When drug exposure time was prolonged to 72 h, melphalan at all doses significantly increased sub-G1 fractions (vehicle vs. 8 μM, p = 0.0006; vehicle vs. 16 μM, p < 0.0001; vehicle vs. 32 μM, p < 0.0001) and concomitantly reduced G0/G1 fractions (vehicle vs. 8, 16, 32 μM; p < 0.0001) (Fig. 5b). Treatment with 8 and 16 μM melphalan induced S-phase arrest (vehicle vs. 8 μM, p = 0.0029; vehicle vs. 16 μM, p < 0.0047), which was similar to 24 h exposure, but was sufficient to stop G2/M-phase entry [vehicle vs. 8 μM, p = 0.0045; vehicle vs. 16 μM, p < 0.0001) (Fig. 5b). This indicated that melphalan at low doses required a longer exposure time for anticancer activities.

Topotecan at 11 μM demonstrated efficiently reduced the number of tumor cells in G0/G1 and G2/M phases (vs. vehicle, p < 0.0001 and p = 0.0237) and simultaneously induced subG1 phase (p < 0.0001) in treated tumor organoids, consistent with the elevated number of CC3+ cells (p < 0.0001) (Fig. 5a–c, g, j). Similar results regarding cell cycle distribution were obtained at 72 h of exposure, while further prolonging the incubation period increased cell death and reduced the number of G0/G1-phase cells (Fig. 5a, b). The S-phase fraction was not different from vehicle-treated organoids at both time points (Fig. 5a, b). This suggests that topotecan differentially targeted G1/G0- and G2/M-phase cells. In addition, topotecan and the highest doses of melphalan showed similar cell cycle profiles (Fig. 5b), resulting in comparable killing effects in treated organoids (Fig. 5c, f, g, j).

Methotrexate induced S-phase arrest and subsequently prevented G2/M-phase entry (vs. vehicle, p = 0.0234 and p = 0.0465) (Fig. 5a, b). However, similar to 8 μM melphalan, the drug was not sufficient to substantially induce cell death at 24 h of exposure, consistent with CC3+ staining (Fig. 5a–d, h, j). Prolonged exposure to methotrexate simultaneously caused a reduction the number of G0/G1-phase cells and increased cell death in sub-G1-phase cells (vs. vehicle, p < 0.0001 and p = 0.0031) while maintaining action in S and G2/M phases (Fig. 5b). This indicated that methotrexate had a slow anticancer effect.

To increase efficiency in controlling tumor growth, combined melphalan and topotecan is used clinically6, but the comparative genotoxic effect of combinatorial drugs, relative to each single drug, has been unknown. Hence, 16 μM melphalan and 11 μM topotecan were tested in tumor organoids. The combined drug regimen significantly reduced S-phase arrest relative to that induced by melphalan alone ($p < 0.0001$), in concert with increased cell death in sub-G1 phase ($p = 0.0105$) (Fig. 5a, b); this was consistent with an elevated number of CC3+ cells ($p = 0.0329$) (Fig. 5e, g, i, j). Cell cycle distribution was generally similar to topotecan alone (Fig. 5b). The number of CC3+ cells in treated organoids indicated that the combined drug regimen and topotecan alone had a comparable killing effect to that of 32 μM melphalan (Fig. 5j). Prolonged exposure to the combined drug regimen caused an increased G0/G1 fraction, relative to that induced by either agent alone, indicative of cell arrest (vs. melphalan, $p = 0.0053$) (Fig. 5b). This subsequently prevented S- and G2/M-phase entry in a significantly greater proportion of cells than melphalan alone ($p = 0.0007$ and $p = 0.0101$) (Fig. 5b). Altogether, this suggested that the genotoxic effect of the combined drug regimen was superior to melphalan alone; however, the combined drug regimen and topotecan alone appeared to have comparable effects in terms of cell cycle distribution and CC3+ staining.

Combined treatment with melphalan and topotecan effectively targets neoplastic cone cells in organoids

Anticancer drugs had a genotoxic effect, as shown by elevated γ-H2AX foci in drug-treated organoids (Fig. S6); this ultimately caused cell death (Fig. 5c–i). Although the combined drugs, topotecan and high-dose melphalan, equally induced cell death (Fig. 5j), viable tumor cells that might be capable of regrowth remained in organoids. We asked whether the remaining cells were proliferative tumor cones and which drugs showed rapid control (at 24 h of exposure) by preferentially destroying proliferative cells, rather than resting tumor cone cells. We labeled RXRγ, which is required for the proliferation and survival of RB12. Co-expression of RXRγ and Ki67 identified proliferative tumor cone cells and differentiated from RXRγ+ Ki67- resting tumor cones (Fig. 6a–u). RXRγ staining indicated that cuboidal or column-shaped cells were maintained as in-vehicle-organoids, suggestive of low efficacy of low and medium doses of melphalan and methotrexate (Fig. 6a, d, g, p). In contrast, organoid cells were transformed into round shapes with the high doses of melphalan, topotecan, and the combined drug regimen (Fig. 6j, m, s). Vehicle-treated organoids consisted of 83.3 ±

2.2% of RXRγ+ cells and 69.2 ± 5.7% of RXRγ+ Ki67+ cells; thus, the cell ratio of RXRγ+ Ki67+ to RXRγ+ was 83.0 ± 5.4% (mean ± SEM) (Fig. 6a–c, v). We found that at 24 h exposure, proportions of viable RXRγ+ cells in drug-treated organoids remained as in-vehicle-organoids (Fig. 6a–v). Topotecan and the combined drug regimen both significantly reduced the proportions of viable RXRγ+ Ki67+ cells (23.5 ± 7.6%, $p = 0.0130$; 20 ± 4.6%, $p = 0.0076$) and cell ratios of RXRγ+ Ki67+ to RXRγ + (48.7 ± 2.0%, $p = 0.0046$; 36.6 ± 3.1%, $p = 0.0003$) (Fig. 6m–o and s–v). This suggested that topotecan, both alone and in combination with melphalan, targeted proliferative tumor cones. In comparison with topotecan alone, the combined drug regimen demonstrated an enhanced effect in reducing proliferative tumor cones (the highest single agent model: CI = 0.74) (Fig. 6w).

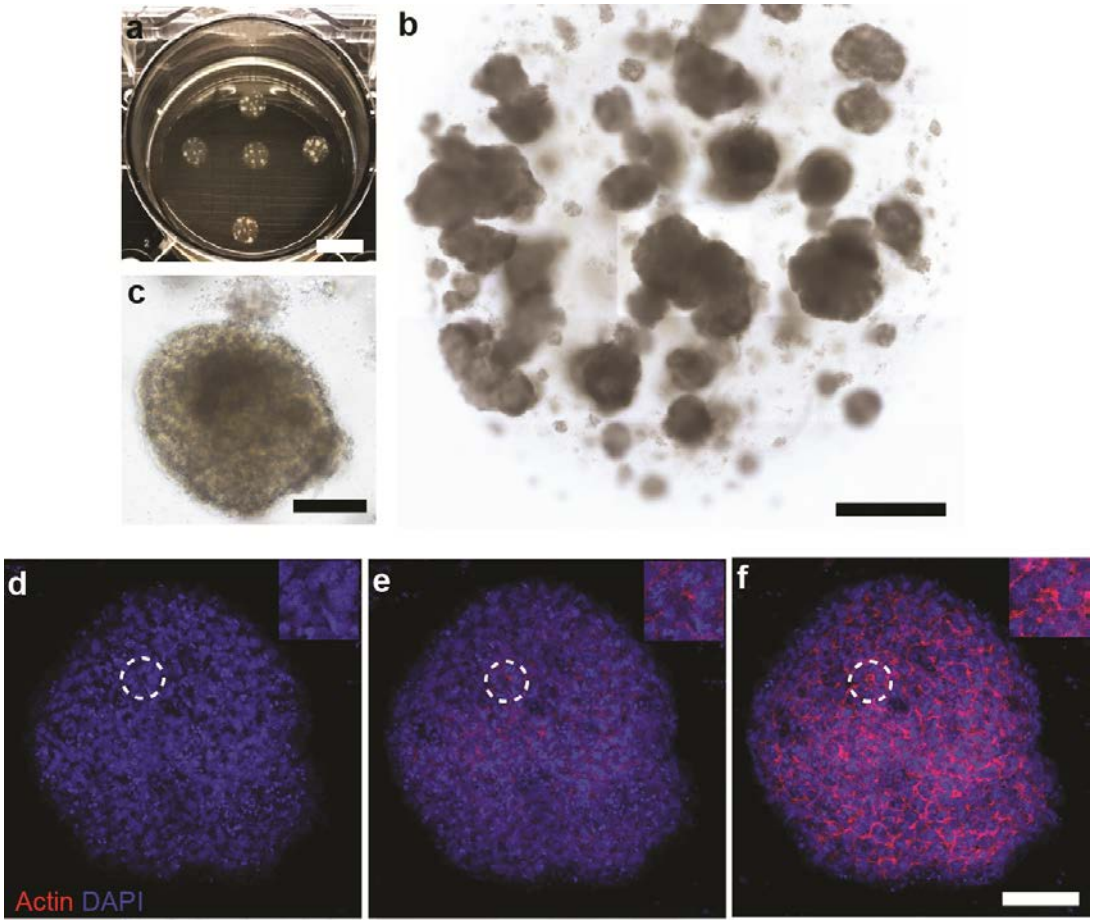

Figure 1. Establishment of retinoblastoma organoid cultures
(a) Photograph of retinoblastoma organoids grown in Matrigel® drops. (b) Mosaic image shows of multiple organoid sizes in a single Matrigel® drop; typical growth features of a 3-week culture after passaging. (c) Magnified micrograph of organoids showing dense cellular organization. (d–f) Confocal z-plane images of whole-mount organoid (bottom to top), stained with phalloidin and 4',6-diamidino-2-phenylindole (DAPI), showing multiple rosette formation (dashed-line circles indicate inserted images). Scale bar, 1 cm (a); 1000 μm (b); 200 μm (c) and 100 μm (d–f).

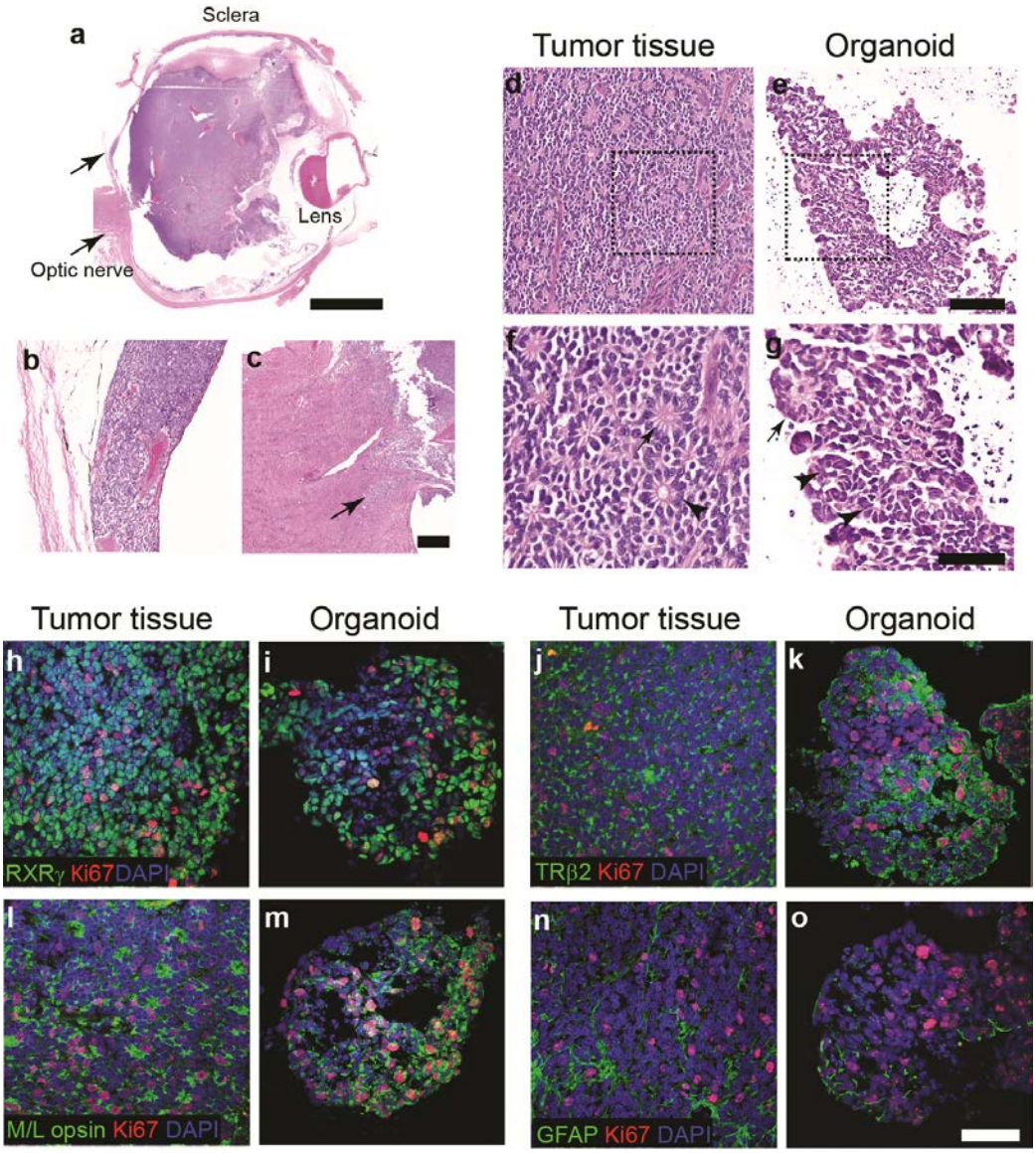

Figure 2. Reproducible cellular features and contents of the retinoblastoma in tumor organoids

(a–c) Hematoxylin and eosin staining of the enucleated globe (a). Arrows in (a) indicate magnified regions showing choroid (b) and optic nerve (c, (arrow)) invasion. (d–g) Representative micrographs indicate histological features of parental tumor tissue (d, e) and organoids (f, g). Dashed-line squares in (d, e) indicate magnified regions presented in (f, g). Flexner-Wintersteiner (arrowhead) and Homer-Wright (arrow) rosettes (f, g) were maintained in organoids. (h–o), Representative micrographs of immunostaining indicate the expression of Ki67 and cone-specific proteins [RXRγ (h, i), TRβ2 (staining specificity demonstrated by Xu et al.12) (j, k), M/L opsin (l, m)] or glial fibrillary acidic protein [GFAP (n, o)] in parental tumor tissue and organoids. Nuclei stained by 4',6-diamidino-2-phenylindole (DAPI). Scale bar, 5 mm (a); 200 μm (b, c); 100 μm (d, e) and 50 μm (f–o). See Fig. S2 for other retinal markers.

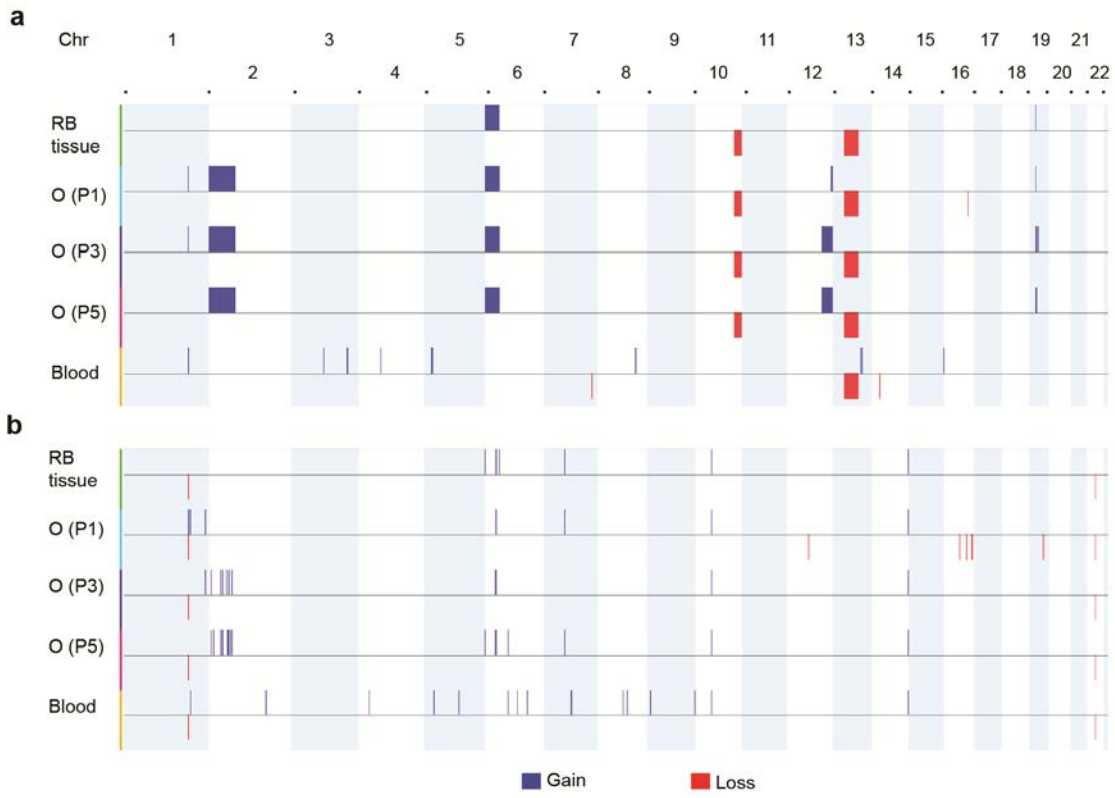

Figure 3. DNA copy number landscape of patient-derived retinoblastoma organoid line
(a, b) Copy number aberration of regional gains and losses (>3 Mb) (a) and focal lesions (<3 Mb) (b) in retinoblastoma (RB) tissue, organoids (O) at passage 1 (P1, 6-week culture), 3 (P3, 13-week culture), and 5 (P5, 19-week culture), matched with peripheral blood. See Fig. S3 for the frequency of gains or losses in tissue and organoids.

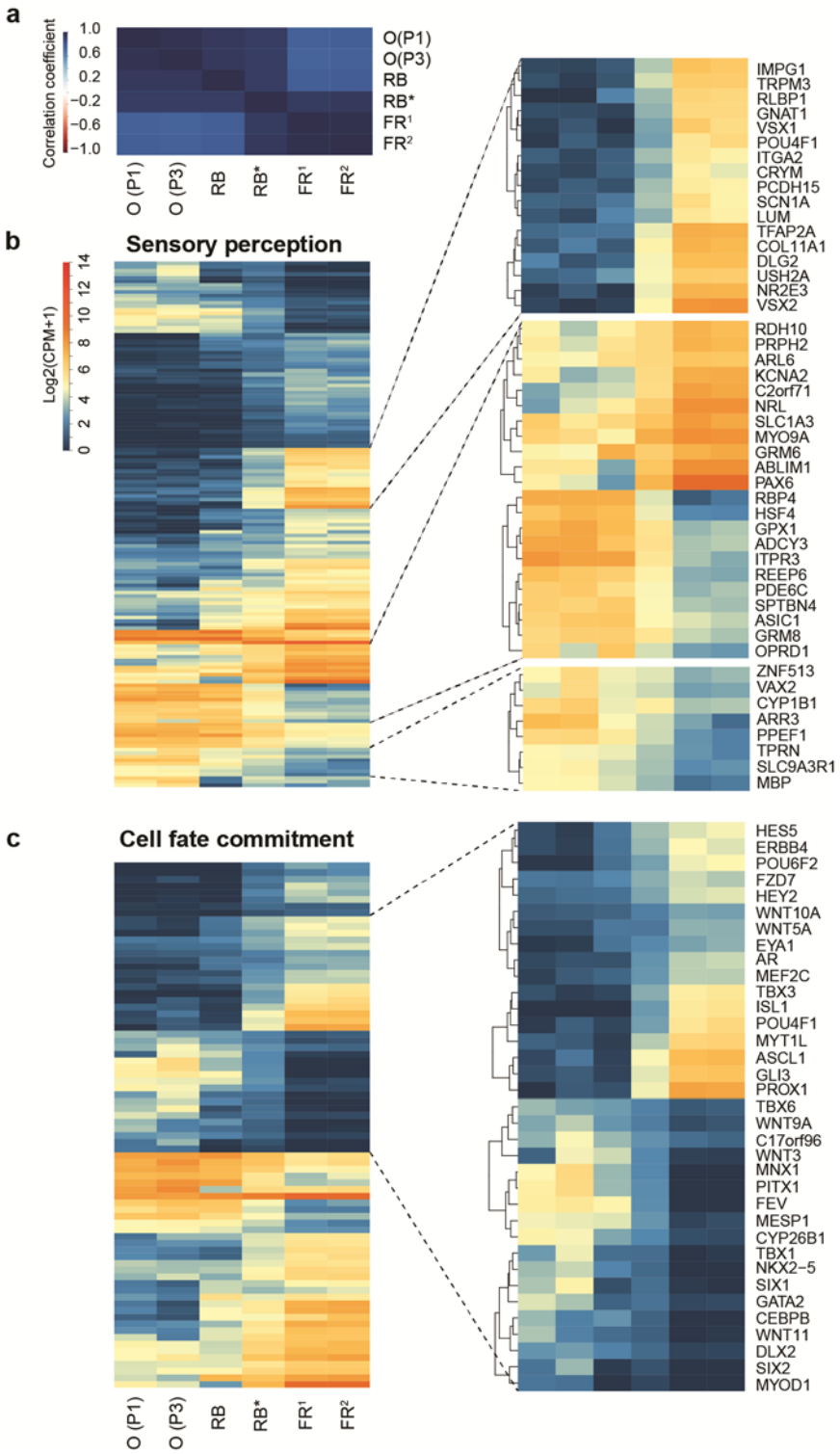

Figure 4. Tumor organoids recapitulate gene expression profile of primary retinoblastoma tissue of origin

(a) Correlation heat map between organoids (O) at passage 1 (P1, 6-week culture) and 3 (P3, 13-week culture), the corresponding patient-derived retinoblastoma (RB) and published transcriptomes of retinoblastoma (RB*) and fetal retina (FR1 and FR2). (b, c) heat maps show differentially expressed genes of the two most significant gene ontologies (GOs), associated with sensory perception (b) and cell fate commitment (c). See Fig. S5 for other GOs and their corresponding gene expression profiles.

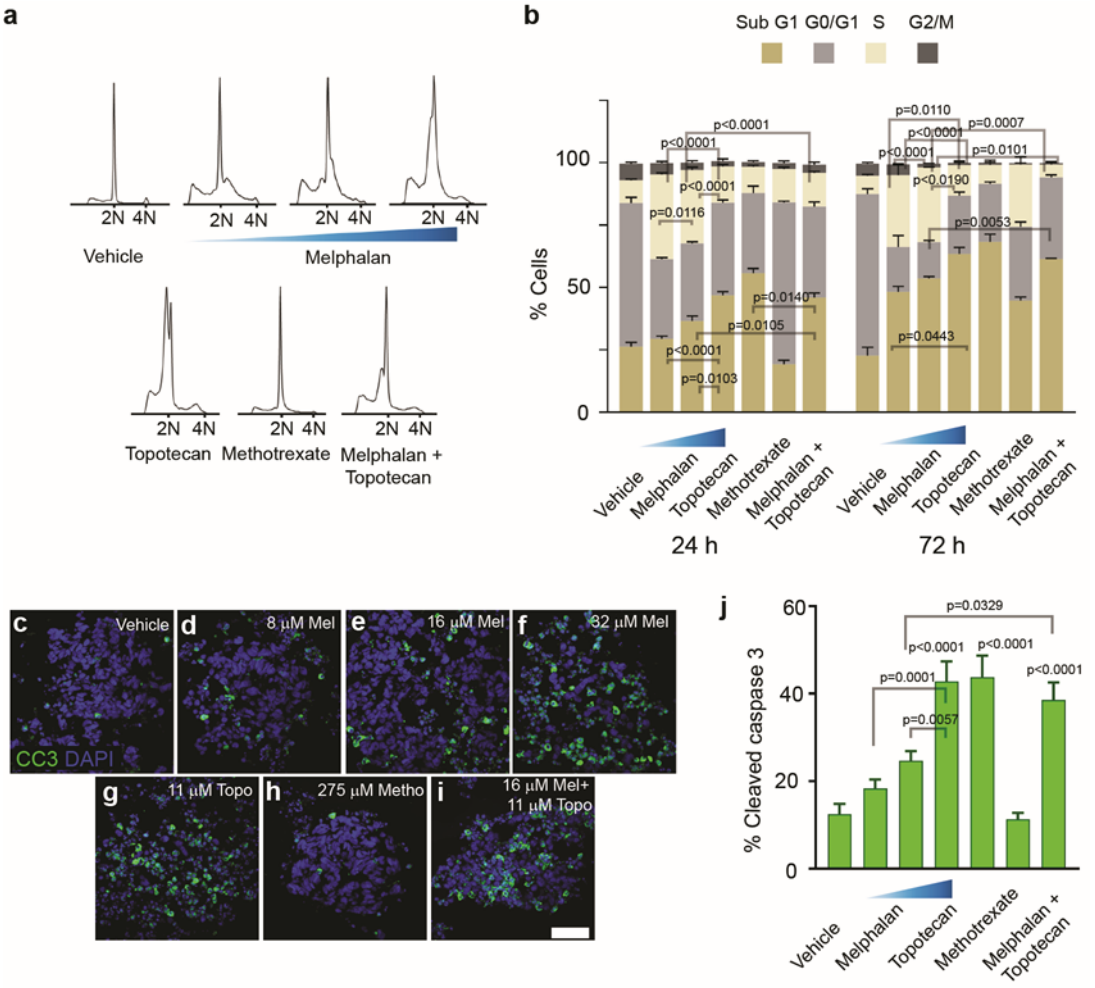

Figure 5. Chemotherapeutic drug responses of tumor organoids
(a, b) Cell cycle analysis of organoids in response to anticancer drugs at 24 (a, b) and 72 (b) h after drug administration. Statistical analysis of cell cycle phases at each time point (mean percentage ± SEM, n=3) was conducted by one-way ANOVA followed by Tukey's test. (c–i) Representative micrographs of immunostaining for cleaved caspase 3 (CC3), an indicative marker of apoptotic cells in organoids treated with vehicle (c), 8 (d), 16 (e), or 32 (f) µM melphalan (Mel), 11 µM topotecan (Topo) (g), 275 µM methotrexate (Metho) (h), or the combined regimen of 16 µM melphalan with 11 µM topotecan (i). Nuclei stained by 4',6-diamidino-2-phenylindole (DAPI). Scale bar, 50 µm. (j) Bar graph indicates % CC3+ cells (mean percentage ± SEM, n=3) after exposure to drugs for 24 h. Mean percentages were determined from 7–10 micrographs containing 300–500 cells for each condition. Statistical analysis of % CC3+ cells was conducted by one-way ANOVA followed by Tukey's test. The p values of single or combined agents vs. vehicle for cell cycle analysis are listed in the text.

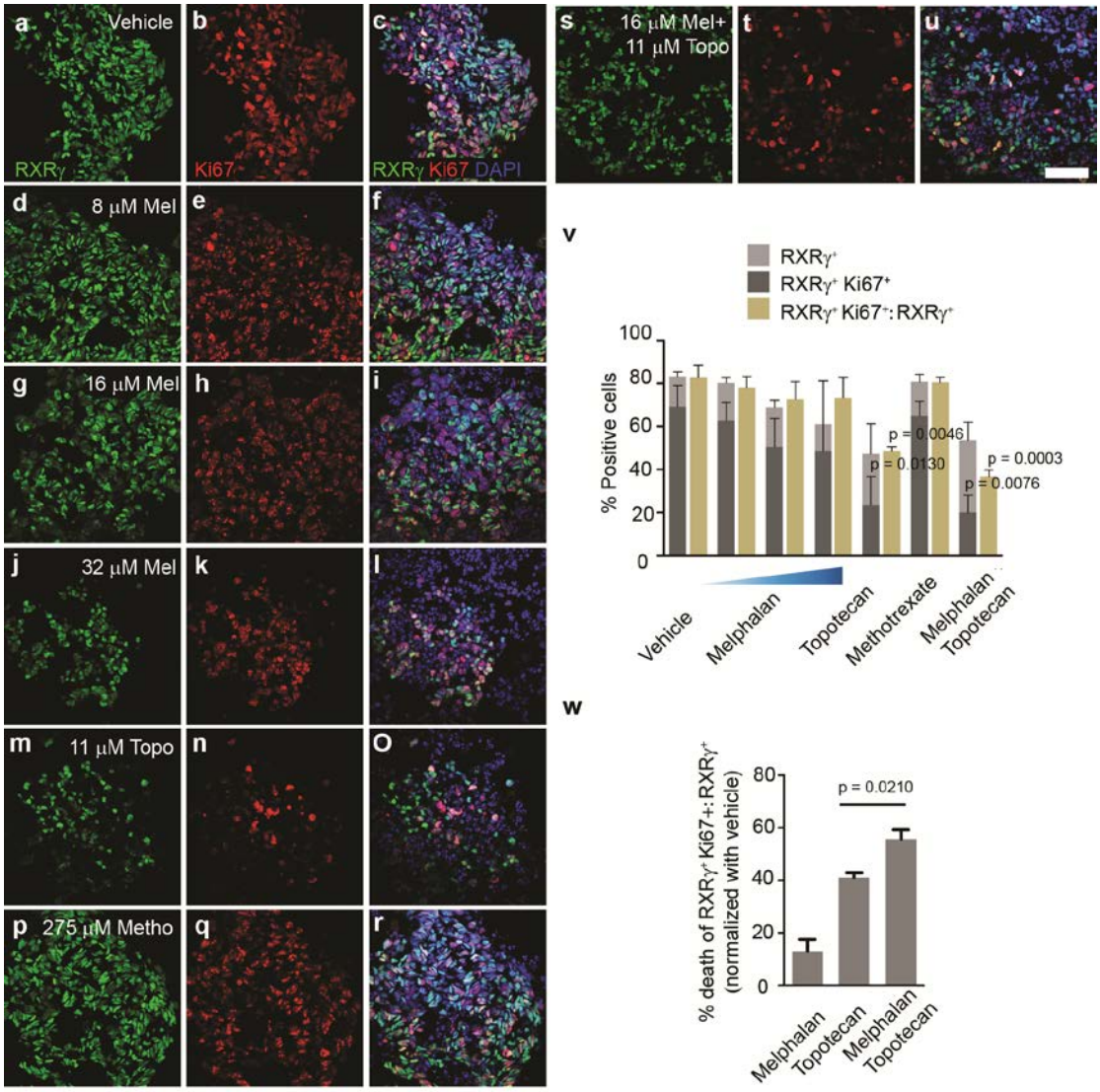

Figure 6. Cone cell features in organoids in response to anticancer drugs at 24 h.
(a–u) Representative micrographs of immunostaining for cone marker RXRγ (a, d, g, j, m, p, and s) and proliferative marker Ki67 (b, e, h, k, n, q, and t) in organoids treated with vehicle (a–c), 8 (d–f), 16 (g–i), or 32 (j–l) μM melphalan (Mel), 11 μM topotecan (Topo) (m–o), 275 μM methotrexate (Metho) (p–r), or the combined regimen of 16 μM melphalan with 11 μM topotecan (s–u). Merged images (c, f, i, l, o, r, and u). Nuclei stained by 4',6-diamidino-2-phenylindole (DAPI). Scale bar, 50 μm. (v) Bar graph shows % RXRγ+ cells (non-proliferative cones), RXRγ+ cells co-stained with Ki67 (proliferative cones), and ratio of proliferative to non-proliferative cones (mean percentages ± SEM, n=3). Mean percentages (proportions) were determined in nine micrographs for each condition. Statistical analysis of % positive cells was conducted by one-way ANOVA followed by Dunnett's test. (w) Bar graph shows death of cell ratio of RXRγ+ Ki67+ to RXRγ+ (mean percentages ± SEM, n=3, unpaired t-test).

4. Conclusion and Discussion

Culture systems greatly impact the maintenance of tumorigenic aspects in primary tumor-derived cells. Two-dimensional adherent cultures, despite being amenable to high-throughput screening, do not recapitulate and rarely represent clinically relevant patient tissues[33]. The advent of organoid cultures has allowed recapitulation of 3-D, self-organizing cellular structures that resemble tissue. Here, we demonstrated that tumor organoids can be derived from a tumor of the retina and can retain molecular and cellular features of the parental tumor. Additionally, as a model of vitreous seeds tumor organoids produced different drug responses that can be used to predict anticancer drug activities for seed control.

Two subgroups of RB with biallelic loss of the RB1 gene have been identified; both exhibit gene expression signatures of cone photoreceptors, although the cone-associated genes are expressed more highly in one group than the other[34]. The reduced expression of cone-associated genes is proposed to associate with increased genomic alterations, which contribute to tumor progression[35]. Consistently, RB organoids in our study exhibited well-preserved cone gene expression signatures and cone-specific proteins, reflective of the tumor cell of origin. In addition, irregular expression of genes associated with mesodermal cell lineage in tumor cells with cone signatures reflects intrinsic properties of RB that possess invasive and metastatic capacities; this indicates that organoids are well-represented vitreous seeds. We detected additional regional gains in organoids, which could represent undetectable genomic disruptions within the original tumors and may coevolve through a Darwinian selection process to increase the fitness of the overall tumor population[36]. These alterations, such as regional 2p gain, have been documented in primary RB[31, 32] and allow the emergence of a complex clonal architecture that may underlie tumor proliferation, progression, or drug resistance.

Analysis of RB1-depleted retinal cells identifies differentiating cones as tumor-initiating cells that form RB-like tumors in orthotopic xenografts[13]. Human cone-specific signaling circuitry sensitizes to cancerous transformation and collaborates with RB1 depletion[12, 13]. An intrinsically high level of expression of the MDM2 proto-oncogene in human cones predisposes them to transformation by preventing cell death[12, 37]. MDM2 expression is regulated by the cone-specific RXRγ, which, together with TRβ2, is required for the proliferation and survival of RB[12, 38]. The expression of MDM2 is not detected in

xenografts[7], but was expressed in our tumor organoids, together with RXRγ and TRβ2. This indicates that organoids retain cone-specific signaling circuitry, suggesting the use of tumor organoids as a model for examining targeted therapies specifically designed to destroy this circuitry.

Organoids provide opportunities for testing the accessibility of therapeutic agents and ex vivo screening of drug sensitivities. We found that combined treatment with topotecan and melphalan was more effective than melphalan alone, consistent with clinical outcomes observed in attempts to control vitreous seeds6. Melphalan (20–30 μg) is extensively used in intravitreal chemotherapy, but in some cases fails to control recurrent and refractory seeds[1, 3]. The combined drug regimen achieves rapid control of seeds, such that fewer cycles of chemotherapy are required, compared with melphalan alone[6]. Because of its limited toxicity[39], topotecan alone has been recently used to manage persistent vitreous seeds with satisfactory outcomes; its efficacy is between that of melphalan alone and the combined drug regimen[4], consistent with our results. Partial control of seeds has been achieved with low-dose melphalan (8–10 μg), consistent with our results. Higher doses of melphalan (>40 μg) cause ocular complications[2]. Unlike other drugs, methotrexate showed slow effects and exhibited the lowest efficacy, consistent with the need for multiple injections over a longer period of treatment[5]. Organoids showed that topotecan alone and in combination with melphalan effectively targeted proliferative cones, rather than non-proliferative cones. Topotecan, a topoisomerase I inhibitor, induces rapid cellular stress in G1, G2, and S phases, thereby causing failure to engage mitosis[40], which is consistent with our results. We routinely used melphalan and methotrexate with variable success in controlling vitreous seeds. The results of the current study are consistent with previous reports[4, 6] that encouraged the use of topotecan and melphalan in management of vitreous seeds.

The tumor microenvironment, or tumor stroma, is highly responsible for growth, metastasis, and drug resistance through paracrine effects[41, 42]. Glial cells with astrocyte properties, which serve as the tumor microenvironment, promote proliferation and survival of RB[43]. Organoids and tumor tissue contained glial cells, as indicated by GFAP+ cell staining, which constitute ∼2–3% of the cells in RB tumors12. The expression of GDNF (by glia or fibroblasts), and its cognate receptor RET, in organoids and the parental tumor (Fig. S5b, c) implies crosstalk between RB glia and tumor cells.

Unlike tumor organoids, GFAP+ cells are absent in tumorspheres derived from RB33, representing a clear advantage of organoids in generating a close-to-patient model.

In the era of precision medicine, faithful preclinical models are important for guiding treatment options. Organoid technology offers simple and efficient generation of 3-D-tumor tissue models. RB organoid models retained cone signal circuitry and produced clinically relevant drug responses, thus facilitate development of targeted therapies that can be used in management of vitreous seeds. As a model, organoids could accelerate the discovery of novel therapies, while reducing animal usage and costs invested in therapeutic development.

References

1. Berry, J.L. et al. Not all seeds are created equal: seed classification is predictive of outcomes in RB. Ophthalmology. 124, 1817–1825 (2017).
2. Ghassemi, F. & Shields, C.L. Intravitreal melphalan for refractory or recurrent vitreous seeding from retinoblastoma. Arch Ophthalmol. 130, 1268–1271 (2012).
3. Shields, C.L. et al. Intravitreal melphalan for persistent or recurrent retinoblastoma vitreous seeds: preliminary results. JAMA Ophthalmol. 132, 319–325 (2014).
4. Rao, R., Honavar, S.G., Sharma, V. & Reddy, VAP. Intravitreal topotecan in the management of refractory and recurrent vitreous seeds in retinoblastoma. Br J Ophthalmol. 102, 490–495 (2017).
5. Kivelä, T., Eskelin, S. & Paloheimo, M. Intravitreal methotrexate for retinoblastoma. Ophthalmology. 118, 1689–1689.e6 (2011)
6. Ghassemi, F., Shield,s C.L., Ghadimi, H., Khodabandeh, A. & Roohipoor, R. Combined intravitreal melphalan and topotecan for refractory or recurrent vitreous seeding from retinoblastoma. JAMA Ophthalmol. 132, 936–941 (2014).
7. McEvoy, J. et al. Coexpression of normally incompatible developmental pathways in retinoblastoma genesis. Cancer Cell. 20, 260–275 (2011).
8. Nair, RM. & Vemuganti, GK. Transgenic models in retinoblastoma research. Ocul Oncol Pathol. 1, 207–213 (2015).
9. MacPherson, D. et al. Cell type-specific effects of Rb deletion in the murine retina. Genes Dev. 18, 1681–1694 (2004).

10. Chen, D. et al. Cell-specific effects of RB or RB/p107 loss on retinal development implicate an intrinsically death-resistant cell-of-origin in retinoblastoma. Cancer Cell. 5, 539– 551 (2004).
11. Aldiri, I. et al. The dynamic epigenetic landscape of the retina during development, reprogramming, and tumorigenesis. Neuron. 94, 550–568.e10 (2017).
12. Xu, X.L.et al. Retinoblastoma has properties of a cone precursor tumor and depends upon cone-specific MDM2 signaling. Cell. 137, 1018–3101 (2009).
13. Xu, X.L.et al. Rb suppresses human cone-precursor-derived retinoblastoma tumours. Nature. 514, 385–388 (2014).
14. Benavente, C.A. et al. Cross- species genomic and epigenomic landscape of retinoblastoma. Oncotarget. 4, 844–859 (2013).
15. Zhang, J. et al. A novel retinoblastoma therapy from genomic and epigenetic analyses. Nature. 481, 329–334 (2012).
16. Dutta, D., Heo, I. & Clevers, H. Disease modeling in stem cell-derived 3D organoid systems. Trends Mol Med. 23, 393–410 (2017).
17. Fatehullah, A., Tan, S.H. & Barker, N. Organoids as an in vitro model of human development and disease. Nat Cell Biol. 18, 246–254 (2016).
18. Hoshino, A. et al. Molecular Anatomy of the Developing Human Retina. Dev Cell. 18, 763–779.e4 (2017).
19. Kaewkhaw, R. et al. Transcriptome dynamics of developing photoreceptors in three-dimensional retina cultures recapitulates temporal sequence of human cone and rod differentiation revealing cell surface markers and gene networks. Stem Cells. 33, 3504–3518 (2015).
20. Kaewkhaw R. et al. Treatment paradigms for retinal and macular diseases using 3-D retina cultures derived from human reporter pluripotent stem cell lines. Invest Ophthalmol Vis Sci. 57, ORSFI1–ORSFI11 (2016).
21. Fujii, M. et al. A colorectal tumor organoid library demonstrates progressive loss of niche factor requirements during tumorigenesis. Cell Stem Cell. 18, 827–838. (2016).
22. van de Wetering, M. et al. Prospective derivation of a living organoid biobank of colorectal cancer patients. Cell. 161, 933–945 (2015).
23. Sachs, N. et al. A living biobank of breast cancer organoids captures disease heterogeneity. Cell. 172, 373–386.e10 (2018).

24. Broutier, L. et al. Human primary liver cancer-derived organoid cultures for disease modeling and drug screening. Nat Med. 23, 1424–1435 (2017).
25. Gao, D. et al. Organoid cultures derived from patients with advanced prostate cancer. Cell. 159, 176–187 (2014).
26. Baker, L.A., Tiriac, H., Clevers, H. & Tuveson, D.A. Modeling pancreatic cancer with organoids. Trends Cancer. 2, 176–190 (2016).
27. Traverso, V., Kinkl, N., Grimm, L., Sahel, J. & Hicks, D. Basic fibroblast and epidermal growth factors stimulate survival in adult porcine photoreceptor cell cultures. Invest Ophthalmol Vis Sci. 44, 4550–4558 (2003).
28. Roberts, M.R., Hendrickson, A., McGuire, C.R. & Reh, T.A. Retinoid X receptor γ is necessary to establish the S-opsin gradient in cone photoreceptors of the developing mouse retina. Invest Ophthalmol Vis Sci. 46, 2897–2904 (2005).
29. Ng, L. et al. Two transcription factors can direct three photoreceptor outcomes from rod precursor cells in mouse retinal development. J Neurosci. 31, 11118–11125 (2011).
30. Corson, T.W. & Gallie, B.L. One hit, two hits, three hits, more? Genomic changes in the development of retinoblastoma. Genes Chromosomes Cancer. 46, 617–634 (2007).
31. McEvoy, J. et al. RB1 gene inactivation by chromothripsis in human retinoblastoma. Oncotarget. 5, 438–450 (2014).
32. Kooi, I.E.et al. A meta-analysis of retinoblastoma copy numbers refines the list of possible driver genes involved in tumor progression. PLoS One. 11, e0153323 (2016).
33. Bond, W.S. et al. Tumorspheres but not adherent cells derived from retinoblastoma tumors are of malignant origin. PLoS One. 8, e63519 (2013).
34. Kapatai, G. et al. Gene expression profiling identifies different sub-types of retinoblastoma. Br J Cancer. 109, 512–525 (2013).
35. Kooi, I.E. et al. Loss of photoreceptorness and gain of genomic alterations in retinoblastoma reveal tumor progression. EBioMedicine. 2, 660–670 (2015).
36. Burrell, R.A., McGranahan, N., Bartek, J. & Swanton, C. The causes and consequences of genetic heterogeneity in cancer evolution. Nature.501, 338–345 (2013).
37. Qi, D-L. & Cobrinik, D. MDM2 but not MDM4 promotes retinoblastoma cell proliferation through p53-independent regulation of MYCN translation. Oncogene. 36, 1760–1769 (2017).

38. Xu, X.L. et al. SKP2 activation by thyroid hormone receptor β2 bypasses Rb-dependent proliferation in Rb-deficient cells. Cancer Research. 77, 6838–6850 (2017).
39. Buitrago, E. et al. Ocular and systemic toxicity of intravitreal topotecan in rabbits for potential treatment of retinoblastoma. Exp Eye Res. 108, 103–109 (2013).
40. Feeney, G.P. et al. Tracking the cell cycle origins for escape from topotecan action by breast cancer cells. Br J Cancer. 88, 1310–1317 (2003).
41. Onion, D. et al. 3-dimensional patient-derived lung cancer assays reveal resistance to standards-of-care promoted by stromal cells but sensitivity to histone deacetylase inhibitors. Mol Cancer Ther. 15, 753–763 (2016).
42. Bremnes, R.M. et al. The role of tumor stroma in cancer progression and prognosis: emphasis on carcinoma-associated fibroblasts and non-small cell lung cancer. J Thorac Oncol. 6, 209–217 (2011).
43. Xu, X.L. et al. Tumor-associated retinal astrocytes promote retinoblastoma cell proliferation through production of IGFBP-5. Am J Pathol. 177, 424–435 (2010).

5. Appendix

- **Supplementary Materials and Methods**
- **Supplementary Figures**
- **Copy of manuscript**

Supplementary Materials and Methods

Histology, immunofluorescence and imaging

Tumor organoids were fixed with 4% paraformaldehyde solution for 15 min, washed with phosphate-buffered saline (PBS) and incubated in 30% (w/v) sucrose overnight, then embedded in OCT compound and snap frozen. Cryosections (10 μm) of tumor organoids were mounted on SuperFrost Plus slides for immunostaining. Retinoblastoma (RB) tissue/organoids were fixed, dehydrated, and embedded in paraffin. Paraffin sections (4 μm) were stained by hematoxylin and eosin for histological analysis. Cryosections of organoids or paraffin sections of RB tissue were stained with primary (overnight) and secondary antibodies. Paraffin sections were deparaffinized and rehydrated, then antigen retrieval was performed by heating at 95–100°C in buffer (10 mM sodium citrate, 0.05% Tween 20, pH 6.0) for 15 min prior to staining.

The following antibodies were used for staining: AP-2 alpha (1:35, mouse, 3B5, DSHB), BRN-3 (1:200, goat, sc-6026), CHX10 (1:200, goat, sc-21690), RXR gamma (1:100, mouse, sc-365252) from Santa Cruz Biotechnology; GFAP (1:50, mouse, G3893, Sigma); H2AX gamma (1: 400, rabbit, 9718S, Cell Signaling); Ki67 (1:100, mouse, 550609, BD Pharmingen™); Ki67 (1:100, rabbit, RB1510P0, Thermo Scientific™ Lab Vision™); M/L opsin and S-opsin (1:5000, rabbit, gift of Dr. Nathan); NRL (1:1000, mouse, gift of Dr. Swaroop); PAX6 (1:400, mouse, PAX6, DSHB); PROX1 (1:1000, rabbit, AB5475, Millipore); Rhodopsin (1:100, mouse, Rho4D2, Gift of Dr. Molday); cleaved caspase3 (1:400, rabbit, 9661, Cell Signaling); phospho-Histone H3 (1:150, rabbit, 9701, Cell Signaling); and TR

antibodies (1:500) included Alexa Fluor 555 Donkey anti-Goat IgG, Alexa Fluor 568 Goat anti-Rabbit IgG, Alexa Fluor 568 Donkey anti-Mouse IgG, Alexa Fluor 488 Goat anti-Rabbit IgG and Alexa Fluor 488 Goat anti-Mouse IgG (Invitrogen). Phalloidin (1:100, Invitrogen) was used for actin staining. Nuclei were counterstained by 4',6-diamidino-2-phenylindole (DAPI). Fluorescent images were acquired by confocal laser scanning microscopy and Z-stacking was performed with NIS-Element AR (Nikon). Mosaic bright-

field images of organoids were captured by Axiovert A1 and assembled by ZEN lite (Carl Zeiss).

Cell cycle analysis

Tumor organoids were dissociated to yield single cells by TrypLE and fixed in cold 70% ethanol for 2 h at -20°C. Organoid cells were stained with propidium iodine (PI) staining solution (50 μg/ml, with 100 μg/ml RNase and 2 mM MgCl2 in PBS) for 30 min before analysis of DNA contents by flow cytometry. Data were acquired by using a BD FACSVerse system set at 10,000 events.

Copy number analysis

DNA was extracted from primary tumor tissues, organoids, or blood by using DNeasy Blood & Tissue Kits (Qiagen). The quality of DNA specimens was confirmed by agarose gel electrophoresis and the concentration was measured with the Qubit dsDNA BR Assay. RB1 mutations were screened in tumor tissue, organoids, and blood by using direct PCR sequencing. Two hundred nanograms of DNA were used for analyses of copy number alterations and loss of heterozygosity, by using the CGH/SNP array (Infinium CytoSNP-850K array, Illumina) in accordance with the manufacturer's instructions; the results were analyzed and visualized with copy number software (Nexus, BioDiscovery).

RNA sequencing

RNA was extracted from primary RB and tumor organoids at P1 and P3 (6 and 13 weeks post-establishment) by using TriPure isolation reagent (Roche Applied Science). The RNA quality and quantity were determined by RNA6000 assay (Agilent). Specimens with an RNA Integrity Number (RIN) > 8.0 were used in this study. RNA Libraries were constructed by using the TruSeq Stranded mRNA LT Sample Prep Kit (Illumina), in accordance with the manufacturer's instructions. RNA sequencing was performed with the Illumina NavaSeq sequencing system (100-bp paired-end reads); an average of 70 million reads were generated for each sample.

RNA-seq quantification and differential expression analysis

High-quality RNA-seq reads were selected by using Trimmomatic (v0.36). Kallisto (v0.43) was used to compute transcript-level counts on the Ensembl V84 transcriptome (coding and non-coding sequences were included to compute index with Kallisto). To compute gene level expression, the "tximport" R package was used. Initially, gene level

count data was TMM (trimmed mean of M-values); it was normalized and then underwent CPM (counts per million) computation. To account for differences in sequencing, we modeled the data with two batches representing poly-A-tail-pulldown vs. total RNA sequencing protocols. We incorporated these batches in our design matrix and implemented a generalized linear modeling approach for differential expression ("estimateDisp," followed by "glmFit" functions in the "edgeR" package). Genes with log2 fold-change of 2 and Benjamini-Hochberg-adjusted p-values $\leq$ 0.01 were selected as differentially expressed genes.

Gene Ontology Analysis

Gene ontology (GO) analysis of differentially expressed genes was performed by using the "enrichGO" function in the "clusterProfiler" R package (v3.6.0) (PMID: 22455463); the list of all expressed genes ($\geq$ 1 CPM in samples of organoid, RB, or normal samples) was used as the universe in the analysis function.

Supplementary Figures

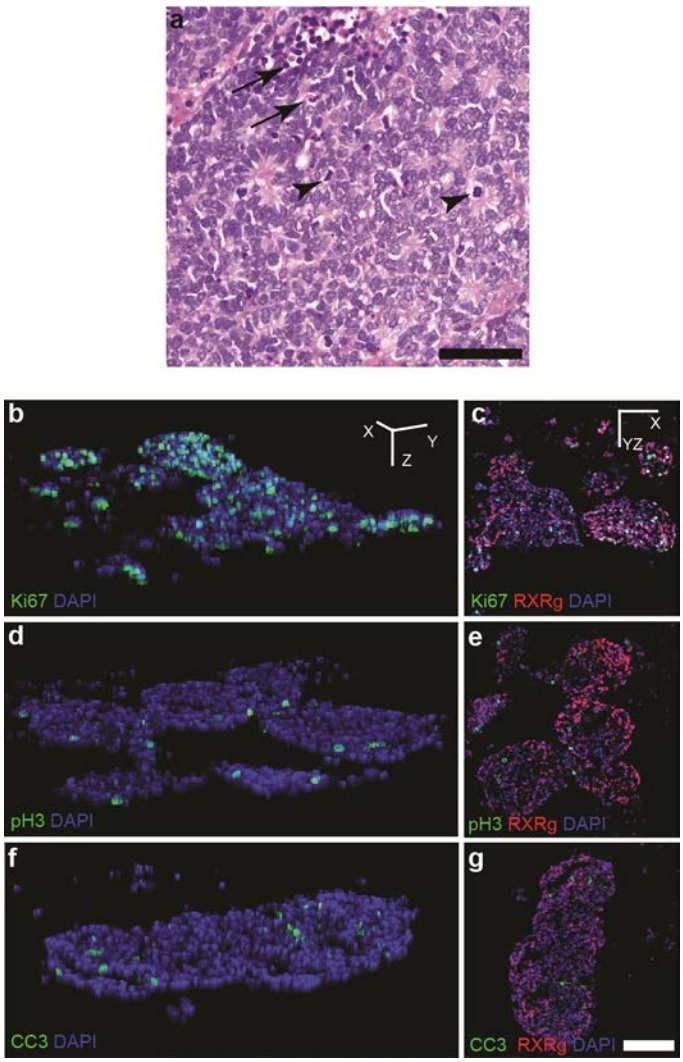

Supplementary Figure 1. Features of proliferative and apoptotic cells in primary retinoblastoma tissue and organoids
(a) Representative micrograph indicating mitotic figures (arrowheads) and apoptotic cells (arrows) in tumor tissue by hematoxylin and eosin staining. (b–g) Immunostaining for proliferative marker Ki67 (b), mitosis-specific marker phospho-histone H3 (pH3) (d) and apoptotic marker cleaved caspase 3 (CC3) (f) co-labeled with cone marker RXRγ (c, e, g). (b, d and f) are three-dimensional visualizations of (c, e, and g), respectively. Nuclei stained by 4',6-diamidino-2-phenylindole (DAPI). Scale bar, 50 μm.

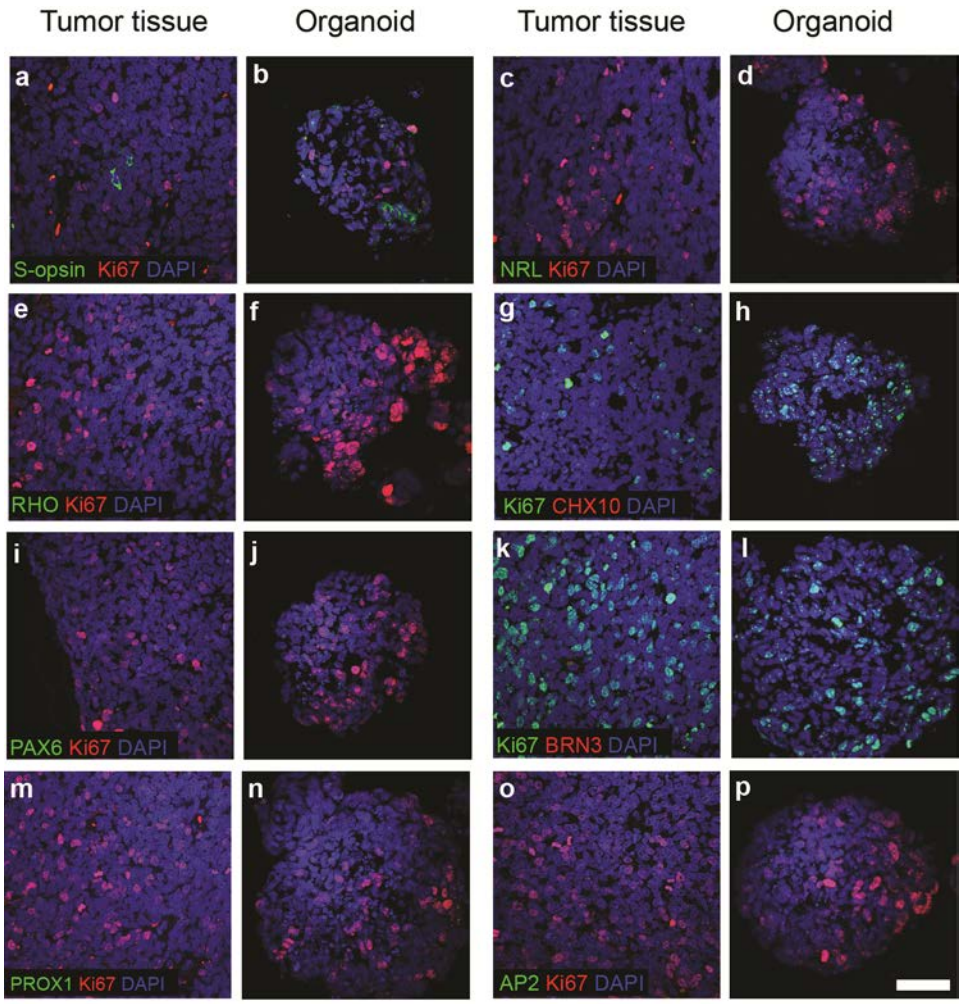

Supplementary Figure 2. Immunostaining for retinal markers in primary retinoblastoma and organoids

(a–p) Representative micrographs of Ki67 co-stained with S-opsin for S cone marker (a, b), NRL (c, d) and RHO (e, f) for rod marker, CHX10 for bipolar/progenitor markers (g, h), PAX6 for horizontal/amacrine/progenitor markers (i, j), BRN3 for retinal ganglia marker (k,l), PROX1 for horizontal/amacrine markers (m, n), and AP2 for amacrine marker (o, p). Nuclei stained by 4',6-diamidino-2-phenylindole (DAPI). Scale bar, 50 μm.

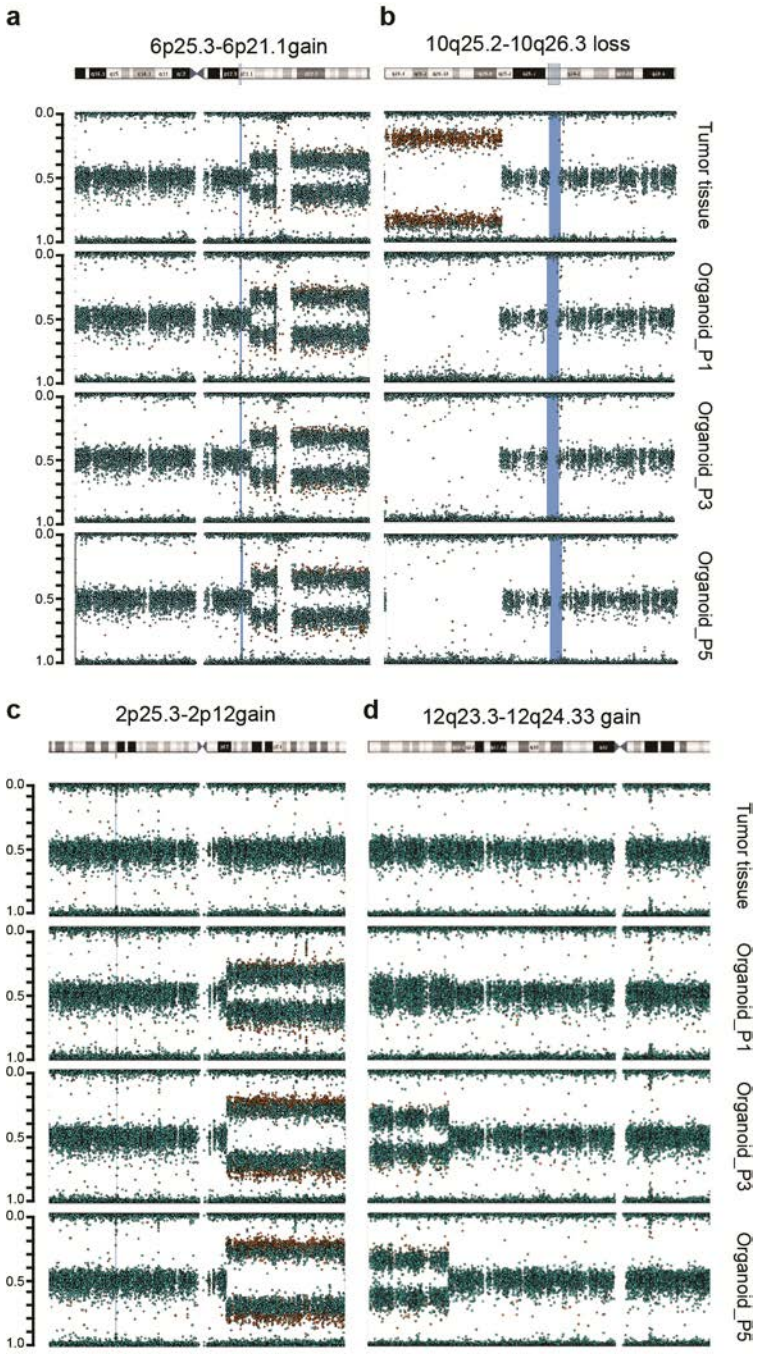

Supplementary Figure 3. Regional recurrent gain or loss found in tumor organoids and tissue

(a–b) B-allele frequency indicates mosaicism of recurrent somatic copy number variation found in tumor organoids at passage 1 (P1, 6-week culture), 3 (P3, 13-week culture), 5 (P5, 19-week culture) and tissue. The sub-clonal neoplastic cells with regional gain at 6p (a) and/or loss at 10q (b) were enriched in tumor organoids. (c–d) B-allele frequency indicates mosaicism of gains at 2p (c) and 12q (d) in organoids. The sub-clonal population with 2p and/or 12q gains increased with additional passaging of organoids. Vertical blue line represents loss of heterozygosity (LOH).

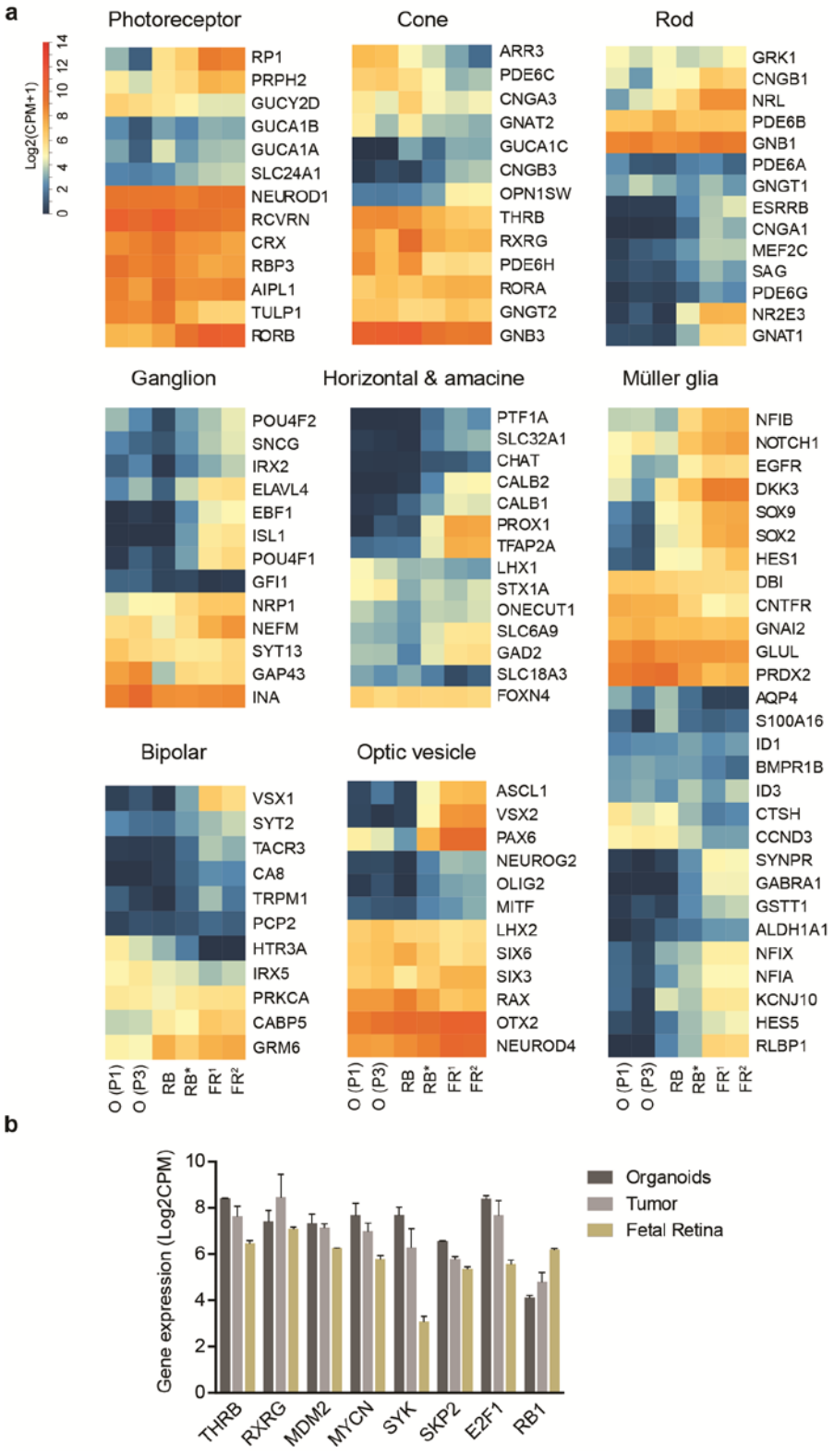

Supplementary Figure 4. Gene signatures representing different retinal cell types
(a) Heat maps show gene expression profiles of organoids (O) at passage 1 (P1, 6-week culture) and 3 (P3, 13-week culture), the corresponding patient-derived retinoblastoma (RB) and published transcriptomes of retinoblastoma (RB*) and fetal retina (FR1 and FR2). (b) Gene expression of cone signal circuitry susceptible to RB transformation in organoids, tumor and fetal retina.

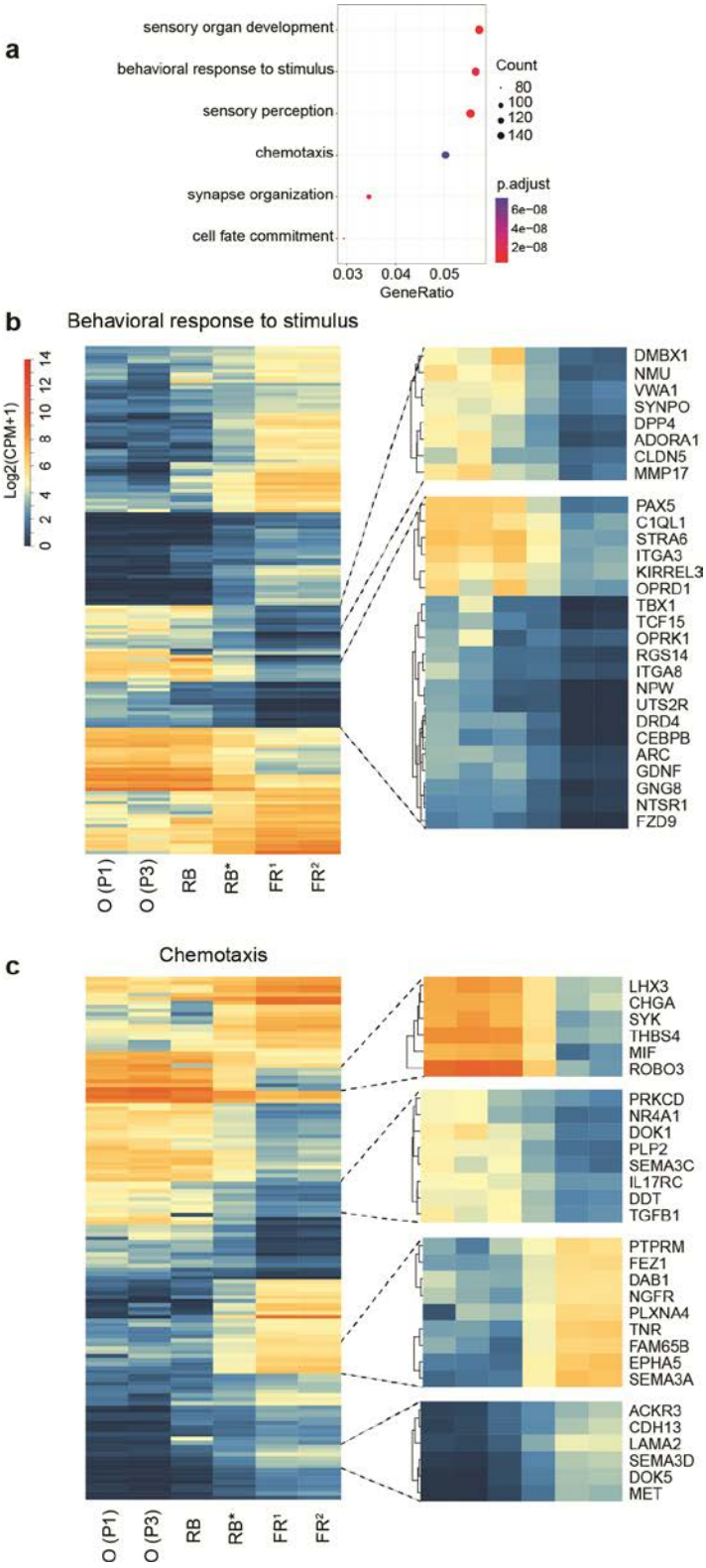

Supplementary Figure 5. Gene ontology (GO) and differentially expressed genes
(a) The six most significant GO terms obtained in a comparison of differentially expressed genes between organoids (O) and fetal retina (FR). (b–c) Heat maps show differentially expressed genes in GOs associated with behavioral response to stimulus (b) and chemotaxis (c).

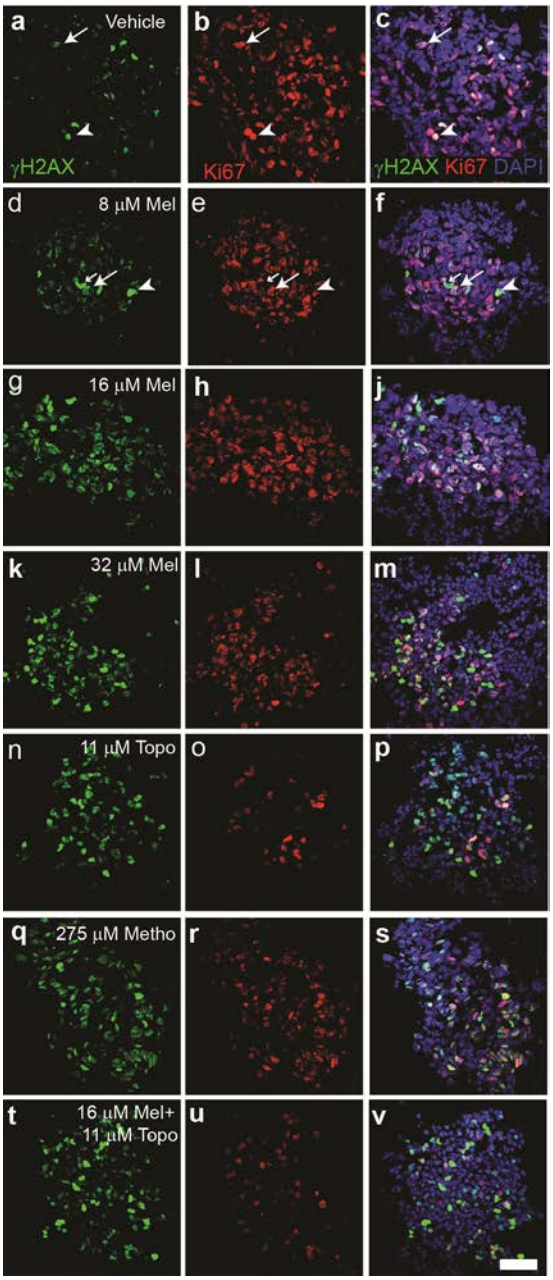

Supplementary Figure 6. DNA damage response after drug administration
(a–v) Representative micrographs of immunostaining for a marker of DNA damage response γH2AX foci (a, d, g, k, n, q, and t) indicate drug accessibility to the core or organoids at 24 h after treatment. Sections were co-labeled with Ki67 (b, e, h l, o, r, and u). Merged images (c, f, j, m, p, s, and v). Organoids treated with vehicle (a–c), 8 (d–f), 16 (g–j), and 32 (k–m) μM melphalan (Mel) , 11 μM topotecan (Topo) (n–p), 275 μM methotrexate (Metho) (q–s) and combined 16 μM melphalan with 11 μM topotecan (t–v). Large arrows indicate organoid cells forming γH2AX foci. Arrowheads (γH2AX+ Ki67+) indicate organoid cells undergoing mitotic γH2AX phosphorylation, whereas small arrows (γH2AX+ Ki67-) indicate apoptotic cells. Nuclei stained by 4',6-diamidino-2-phenylindole (DAPI). Scale bar, 50 μm.

Copy of manuscript

6. Outputs (Acknowledge the Thailand Research Fund)

6.1 International Journal Publications

Two manuscripts were submitted and under reviewed.

- A three-dimensional organoid model recapitulates tumorigenic aspects and drug responses of vitreous seeds in human retinoblastoma (Scientific Reports)
- Spectrum of germline RB1 mutations and clinical manifestations in Thai retinoblastoma patients (Experimental Eye Research)

6.2 Research Utilization and Application

Retinoblastoma organoids will be used for screening of candidate anticancer drugs and developing of targeted therapies for advanced retinoblastoma at Excellent Center for Drug Discovery (ECDD) which has established by the collaborative efforts of Thailand Center of Excellence for Life Sciences (TCELS), Faculty of Medicine Ramathibodi Hospital and Faculty of Science Mahidol University.

A three-dimensional organoid model recapitulates tumorigenic aspects and drug responses of vitreous seeds in human retinoblastoma

Duangporn Seangwimol[1], Duangnate Rojanaporn[2], Vijender Chaitankar[3], Pamorn Chittavanich[4], Rangsima Aroonroch[5], Tatpong Boontawon[4], Weerin Thammachote[4], Natini Jinawath[4], Suradej Hongeng[6] and Rossukon Kaewkhaw[*, 4]

[1]Research Center, [2]Department of Ophthalmology, [4]Section for Translation Medicine, [5]Department of Pathology and [6]Department of Pediatrics, Faculty of Medicine Ramathibodi Hospital, Mahidol University, Bangkok, Thailand. [3]Bioinformatics Computational Biology Core, National Heart, Lung, and Blood Institute (NHLBI), National Institutes of Health (NIH), Bethesda, USA.

[*]Corresponding author: Rossukon Kaewkhaw, Mahidol University, Faculty of Medicine Ramathibodi Hospital, Research Center, Section for Translational Medicine, Floor 3, Bangkok, 10400, Thailand. Phone: 66-201-2615; Fax: 66-201-02971137; E-mail: ross.kaewkhaw@gmail.com and rossukon.kae@mahidol.ac.th.

Abstract

Persistent or recurrent vitreous seeds in advanced retinoblastoma are a major cause of therapeutic failure as a result of drug resistance. This necessitates the development of novel therapies and thus requires a model of vitreous seeds for testing candidate therapeutics. To this aim, we established and characterized a three-dimensional, self-organizing tumor organoid model derived from chemotherapy-naïve primary tumor tissue. The responses of tumor organoids to drugs with final clinical doses achieved in vitreous were determined and compared to relate organoid model to the seeds, in terms of drug sensitivities. We found that tumor organoids preserved histogenesis, DNA copy-number alterations, as well as gene and protein expression of the parental tissue. Cone signal circuitry (M/L^+ cells) and glial tumor microenvironment ($GFAP^+$ cells) were primarily present in organoids. Topotecan alone or the combined drug regimen of topotecan and melphalan effectively targeted proliferative tumor cones ($RXR\gamma^+$ $Ki67^+$) in organoids after 24 h exposure to drugs, blocking mitotic entry. In contrast, methotrexate showed the least efficacy against tumor cells. The results suggest that the responses of organoids were consistent with those of vitreous seeds. Patient-derived tumor organoids enable the creation of a faithful model to use in examining novel therapeutics for vitreous seed control.

Introduction

Retinoblastoma (RB) is a serious childhood retinal tumor that, if left untreated, can cause death within 1–2 years. Current management of RB aims to salvage both the globe and visual function, in addition to saving the patient's life. However, persistent or recurrent vitreous seeds in advanced intraocular RB are a major cause of RB therapeutic failure, representing the primary limitation for globe salvage[1]. Systemic intravenous chemotherapy encounters difficulty in controlling vitreous seeds that exhibit massive and diffuse infiltration, finally leading to enucleation[1]. The minimal response to chemotherapy is partly because of non-vascularization in the vitreous, causing reduced concentration of delivered drugs in the vitreous.

In additional to primary treatment intravitreal chemotherapy is locally applied to increase drug accessibility and shows impressive control of seeds with minimal complications[2, 3]. Melphalan is extensively used despite its high toxicity[2, 3]; this therapy results in an overall globe salvage rate of 68%[1]. A few drugs, such as topotecan and methotrexate, have been used with variable degrees of success[4, 5]; the combination of topotecan and melphalan is optional for refractory and recurrent vitreous seeds[6]. However, case reports have shown failure in some patients, leading to enucleation[1-5]. This highlights the need for drug development and evaluation to ascertain efficacy and safety. Representative and robust models of vitreous seeds are thus required to determine the activities of candidate therapeutic agents for seed control.

Genetically engineered mouse models (GEMMs) are powerful tools to study pathogenesis and develop new therapies for RB[7, 8]. Unlike in human RB, additional

genes must be inactivated together with *Rb1* to induce tumorigenesis in mice[8-10]. Molecular and cellular analyses indicate that mouse RB has properties of amacrine/horizontal interneurons, reflective of the tumor cells of origin[7, 10, 11]. In contrast, cones are frequently identified in human RB[12] and significantly sensitive to cancerous transformation when the *RB1* gene is lost in the human retina[13]. Furthermore, the epigenetic landscape significantly differs between mouse and human RB[11, 14]. Some candidates for molecular targeted therapy, such as epigenetically deregulated *SYK*[15] in human RB, appear to be normally regulated in GEMMs[14]. This indicates that different mechanisms underlying tumorigenesis exist between humans and mice.

Advances in organoid technology allow the generation of three-dimensional (3-D), self-organizing tissue that encompasses multiple lineages through a nature-mimicking process. Accordingly, human and murine organoids have been generated from pluripotent or tissue stem cells in both healthy and diseased conditions[16] and then used to facilitate better understanding in biology and pathology[17-20]. Solid tumor tissues from patients have been used to generate organoids that retain molecular and histopathologic features of the original primary tumor tissue. This has been demonstrated in colon[21, 22], breast[23], liver[24], prostate[25], and pancreatic tumors[26], but has not yet been demonstrated for retinal tumors. Here, we aim to establish model of vitreous seeds through organoid culture derived from enucleated RB tissues for drug testing. Cellular and molecular features are thoroughly characterized to ascertain the presentation of tumorigenic aspects of the parental tumors in organoids after short and long-term culture. As a proof-of-concept of vitreous seed model, we determine and compare the responses of tumor organoids to clinically used drugs for intravitreal chemotherapy[1-6] to relate organoid model to the seeds, in term of drug sensitivities. We further demonstrate that drugs with greater efficacy not only induce cell death,

but also preferentially target proliferative tumor cones, rather than resting cones. Thus, organoids provide opportunities for drug testing and the development of targeted therapies for vitreous seed control in advanced RB.

Results

Establishment of expansible RB organoids

Fresh surgical specimens of chemotherapy-naïve RB were obtained and processed for organoid derivation (~0.3 cm^3 tissue), as well as genomic and transcriptomic analyses. Tissue was mechanically and enzymatically dissociated; dissociated cells were mixed in Matrigel® solution and plated as adherent Matrigel® drops which were overlaid with culture medium. We initially attempted to grow tumor organoids in medium (insulin, transferrin, N2, and FBS) for retinal organoids derived from pluripotent stem cells[19], which failed to support the growth. We then used mitogens (EGF and FGF2, known to support the survival of retinal cells[27]), serum replacement, and culture medium supporting the growth of neural progenitors. This newly formulated medium supported the proliferation of patient-derived cells that previously failed to grow (data not shown). Hence, we used newly formulated medium, in combination with Matrigel®, to establish tumor organoid cultures from the RB tissues of a new patient. This method efficiently allowed generation of tumor organoids and long-term expansion (>8 passages). A cluster of cells initially formed in Matrigel®, then enlarged and became dense and solid (Fig. 1a–c). Organoids were present in multiple sizes up to 1 mm in each single drop of Matrigel® at 3 weeks post-seeding; the cultures could be serially expanded with a consistent passaging ratio of 1:3–1:4 (Fig. 1a and 1b). Individual organoids displayed dense cellular organization of elements resembling rosette formation (Fig. 1c–f). In addition, RB organoids could be

stored and resurrected from long-term storage in liquid nitrogen (up to 5 months' storage was tested) and retained normal cellular structure (data not shown).

RB organoids maintain cellular features of parental tumor

Histological analysis revealed that patient-derived RB tissue filled almost the entire globe and displayed massive choroidal and laminar optic nerve invasion (Fig. 2a–c). The parental RB demonstrated cuboidal cells with hyperchromatic nuclei and scant cytoplasm; this morphology was also found in tumor organoids (Fig. 2d–g). Tumor cells in a circular arrangement, with polarization of the cytoplasm toward the central lumen, indicated the formation of Flexner-Wintersteiner rosettes in organoids, resembling parental tumor tissue (Fig. 2f–g). The presence of Homer-Wright rosettes with neuropil in the lumen, as in primary tumors, was also identified in tumor organoids (Fig. 2f–g). In addition, mitotic figures were frequently present while apoptotic cells were distributed in an irregular fashion among viable cells in primary tumor tissue (Fig. S1a). This was consistent with features of tumor organoids, in which $Ki67^+$ cells were widely distributed among dividing cells at the rim of organoids (Fig. S1b–e). $CC3^+$ cells indicated that apoptosis occurred sporadically in organoids (Fig. S1f, g).

To determine cellular phenotypes, retinal cell and Ki67-proliferative markers were co-labeled in tumor organoids and the corresponding patient-derived tissue (Fig. 2h–o). This co-labeling enabled identification of a specific type of retinal tumor cell, which had the capability of neoplastic growth. Immunostaining revealed that retinoid X receptor-γ (RXRγ) and thyroid hormone receptor β2 (TRβ2), transcription factors important for the differentiation and maintenance of M/L cone identity[28, 29], were detected in a majority of tumor cells within tissues and organoids (Fig. 2h–k). A

subset of RXRγ$^+$ and TRβ2$^+$ cells was co-labeled with Ki67 (Fig. 2h–k). Detection of M/L opsin$^+$ cells and M/L opsin$^+$ Ki67$^+$ cells confirmed the presence of neoplastic M/L cones in primary tissue and organoids (Fig. 2l, m). In contrast, S opsin$^+$ cells were rarely detected and did not express Ki67 (Fig. S2a, b), suggesting that S opsin$^+$ cells are non-proliferative. The expression of rod cell markers (neural retina-specific leucine zipper protein (NRL) and rhodopsin) was not detected in organoids and parental tumor tissue (Fig. S2c–f). In addition to photoreceptors, we examined organoids and their corresponding RB tissue for the expression of other retinal cell markers (Fig. S2g–p). Glial fibrillary acidic protein (GFAP)$^+$ Ki67$^-$ cells were detected, suggesting the presence of non-proliferative glial cells in tumor organoids, similar to parental tumor tissue (Fig. 2n, o). In contrast, retinal progenitor (CHX10 and PAX6), ganglion (BRN3 and PAX6), bipolar (CHX10), amacrine (PROX1, AP2-α, and PAX6), and horizontal (PROX1 and PAX6) cells were absent, a finding that concurred with data from tumor tissue (Fig. S2g–p). Altogether, the results demonstrated that RB organoids recapitulated and retained the histological characteristics and retinal protein expression of the parental tumor tissue. Detailed analysis also indicated that neoplastic cells retained M/L cone phenotypes, even after long-term expansion in culture or storage in liquid nitrogen, in the same culture conditions (data not shown).

RB organoids retain genetic alterations of original tumor tissue

While the initiation of RB occurs as a result of *RB1* biallelic loss, recurrent genomic gains and losses drive tumor progression. These alterations were determined in organoid cultures at 6 (P1), 13 (P2), and 19 (P5) weeks, in comparisons of tumor tissue matched with peripheral blood. Screening for *RB1* mutations identified a large deletion (13q13.1–13q22.2) spanning the *RB1* gene (Fig. 3a) as a germline mutation. An additional mutation (g.41924A>G) in retinal cells that became cancerous

transformation resulted in defective splicing of *RB1* transcripts. The biallelic loss of *RB1* was present in patient-derived organoids (Fig. 3a). The recurrent regional gains (>3 Mb) were consistently identified at 6p25.3–6p21.1 and 19p12–p11; losses occurred at 10q25.2–10q26.3 in parental tumor and organoids at different serial passages (Fig. 3a). In addition, recurrent copy number aberrations were frequently found in tumor organoid cells, indicating that sub-clonal populations found in tumor tissue were enriched in organoids; this was consistently maintained with serial passaging (Fig. 3 and S3a, b).

Two additional large regional gains (2p25.3–2p12 and 12q23.3–12q24.33) were identified in organoids (Fig. 3a and S3c, d); sub-clonal populations with these gains were further enriched with serial passaging (Fig. S3c, d). In addition, focal lesions (<3 Mb) were detected within the same fragments, with large regional gains consistently identified at chromosomes 2 and 6 and inconsistently identified at chromosome 16 (Fig. 3b). Somatic copy number alterations, including 1q, 2p, and 6p gains, as well as 16q loss, are commonly identified in RB[30, 31]. In addition, the recurrent 6p gain is associated with 2p gain, while the 1q gain is associated with 16q loss; the former association precedes the latter and thus is identified in RB tumors from patients diagnosed at younger age[32]. This suggests that 2p gain could be expected in organoid cells that were derived from the tumor with the recurrent 6p gain in our young patient at 7 months of age at diagnosis. Loss of heterozygosity was consistently maintained between tissue and organoids at different passages (data not shown).

Gene expression profile reflects the origin of RB in tumor organoids

Gene expression profiling from RNA-seq data was conducted to determine whether tumor organoids retain a gene signature of the parental tumor, reflecting the

histogenesis of RB. Since the tumor was diagnosed at early age (7 months) in our RB patient, we included published transcriptome data of fetal retina (19 weeks)[18] and RB[11] for analysis (Fig. 4, S4, S5). Gene profiling analysis revealed that tumor organoids strongly correlated with the parental tumor tissue and were consistent between passages (Fig. 4a). As expected, the gene signatures indicated that the organoids and tumor tissue had a higher degree of correlation with primary RB than with normal developing retina (Fig. 4a). Furthermore, gene expression profiles of our samples were more readily distinguishable from normal retina (Fig. 4a) than in reported cases of RB, suggesting a higher purity of tumor cellularity in our samples. Transcriptomes of retina-enriched genes demonstrated that tumor organoids and the patient's tumor had high expression levels of cone-enriched genes (Fig. S4a), consistent with the analysis of protein expression. In addition, cone-associated genes that are susceptible to RB transformation were upregulated in tumor tissue and organoids, in response to *RB1* inactivation (Fig. S4b).

Functional annotation of differentially expressed genes between tumor organoids and fetal retina revealed that enrichment for the gene ontology (GO) associated with sensory perception was the most significant (Fig. 4b, S5a). We found that downregulated genes in organoids and tumor tissue, compared with fetal retina, were associated with the development and function of retinal neurons [ganglion (*POU4F1* (*BRN3A*), *KCNA2*, and *SCN1A*), horizontal and amacrine (*TFAP2A* (*AP2-*α) and *PAX6*), and bipolar (*VSX1* and *GRM6*) cells], Müller glial (*RLBP1* and *SCL1A3*) and retinal progenitor (*VSX2* and *PAX6*) cells (Fig. 4b). In addition, rod-enriched genes, including *NRL*, *NR2E3*, *CNGA1*, and *PDE6G*, were downregulated in tumor, but highly expressed in normal retina, where rods outnumber cones (Fig. 4b). In contrast, cone-enriched genes (*PDE6C* and *ARR3*) were upregulated in tumor tissue and further enriched in tumor organoids (Fig. 4b).

Furthermore, cell fate commitment was enriched as the second most significant GO (Fig. 4c, S5a). Concomitantly, we found that cell fate regulatory genes in retinal neuronal lineages were downregulated in tumor organoids and tissue, compared with fetal retina. These included early expressed genes in retinal development (*TBX3*, *PAX6*, *NR2E1*, *EYA1*, and *GLI3*) and regulatory genes for maintaining the retinal progenitor program (Notch signaling: *HES5* and *HEY2*). Similarly, downregulation was detected for genes directing neurogenesis (*ASCL1* and *MYT1*) and the formation of more specific retinal cell types [horizontal and amacrine (*PROX1*), ganglion (*ISL1*, *POU4F1*, and *POU6F2*) and rod (*MEF2C*) cells] (Fig.4c). However, we found that a set of regulatory genes governing mesodermal cell lineage was up-regulated in tumor organoids and tissue, compared with normal retina (Fig. 4c). These genes were normally expressed in developing mesoderm (*TBX6*, *WNT11*, *PITX1*, *FEV* and *CYP26B1*). Likewise, a set of genes functioning in the specification of mesodermal cells (*MESP1*, *TBX1*, *NKX2.5*, *SIX1*, *SIX2*, *GATA2*, and *MYOD1*) was enriched in organoids and tissue (Fig. 4c). Altogether, this suggested that tumor organoids contained hybrid gene signatures for both cone and mesodermal cells. Furthermore, tumor invasion-associated genes (*MMP17* and *ITGA3*) were upregulated in tumor organoids and tissue (Fig. S5a, b). A similar phenomenon was observed for the expression level of *SYK*, contributing to tumor progression after *RB1* inactivation[15] (Fig. S5a, c). A set of genes (*MIF*, *THBH4*, *TGFB1*, *DDT*, *NR4A1*, and *PRKCD*) implicated in the proliferation and invasion of tumor cells was upregulated, whereas genes (*SEMA3A*, *PLEXNA4*, *EPHA5*, and *NGFR*) functioning in normal axonal growth and guidance were downregulated in our samples (Fig. S5c). This was indicative of the invasive and metastatic capacities of tumor organoids, consistent with the metastatic characteristics of the primary tumor (Fig. 2a–c).

RB organoids allow in vitro evaluation of the clinical activity of anticancer drugs for vitreous seed control

To determine whether drug responses of vitreous seeds are reproduced in organoids tumor organoids were treated with clinically used drugs for intravitreal chemotherapy (melphalan, topotecan, and methotrexate). Furthermore, comparisons were made between combined drug (melphalan and topotecan) and single drug regimens, which are challenging to systematically perform in clinics. Concentrations of drugs used in this study were equivalent to the final clinical dose achieved in the vitreous. Since tumor organoids exhibited cellular structure similar to tumor tissue (Fig. 1d–f), we demonstrated that drug accessibility and uptake occurred in the deepest area at the core of tumor organoids, indicated by elevated γ-H2AX foci, a DNA damage response marker (Fig. S6).

Cell cycle profiles (Fig. 5a, b) and apoptosis (Fig.5c–j) were determined in response to anticancer drugs for short (24 h) and long (72 h) exposure times. Melphalan, a common clinical therapy for vitreous seed control, was examined at different doses. Melphalan at 8 µM significantly reduced the number of G0/G1-phase cells ($p < 0.0001$) and induced S-phase arrest ($p < 0.0001$) (Fig. 5a, b). However, this concentration was not sufficient to cause significant cell death, as there was no alteration in the number of sub-G1 and $CC3^+$ cells in treated organoids (Fig. 5a-d, j). Higher concentrations of melphalan (16 and 32 µM) significantly induced elevated sub-G1 fractions (vs. vehicle, $p = 0.0048$ and $p < 0.0001$) (Fig.5a, b), consistent with $CC3^+$ staining for 32 µM melphalan (vs. vehicle, $p < 0.001$) (Fig. 5c, e, f, j). Elevated sub-G1 correlated with reduction of G0/G1 fractions (vs. vehicle, $p < 0.0001$) for both 16 and 32 µM concentrations of melphalan. The effect was more deleterious for the highest dose, reducing the G2/M-phase fraction (vs. vehicle, $p = 0.0277$) (Fig. 5a, b).

Unlike 8 and 16 µM melphalan, tumor organoid cells treated with 32 µM melphalan did not arrest in S phase, but underwent apoptosis in sub-G1 phase (8 vs. 32 µM, $p < 0.0001$; 16 vs. 32 µM, $p = 0.0103$) (Fig. 5a, b), consistent with $CC3^+$ staining (8 vs. 32

μM, p = 0.0001; 16 vs. 32 μM, p = 0.0057) (Fig. 5j). This suggested that after 24 h of exposure, 8 and 16 μM melphalan preferentially induced S-phase arrest; in contrast, 32 μM melphalan immediately targeted tumor organoid cells. When drug exposure time was prolonged to 72 h, melphalan at all doses significantly increased sub-G1 fractions (vehicle vs. 8 μM, p = 0.0006; vehicle vs. 16 μM, p < 0.0001; vehicle vs. 32 μM, p < 0.0001) and concomitantly reduced G0/G1 fractions (vehicle vs. 8, 16, 32 μM; p < 0.0001) (Fig. 5b). Treatment with 8 and 16 μM melphalan induced S-phase arrest (vehicle vs. 8 μM, p = 0.0029; vehicle vs. 16 μM, p < 0.0047), which was similar to 24 h exposure, but was sufficient to stop G2/M-phase entry [vehicle vs. 8 μM, p = 0.0045; vehicle vs. 16 μM, p < 0.0001) (Fig. 5b). This indicated that melphalan at low doses required a longer exposure time for anticancer activities.

Topotecan at 11 μM demonstrated efficiently reduced the number of tumor cells in G0/G1 and G2/M phases (vs. vehicle, p < 0.0001 and p = 0.0237) and simultaneously induced subG1 phase (p < 0.0001) in treated tumor organoids, consistent with the elevated number of $CC3^+$ cells (p < 0.0001) (Fig. 5a–c, g, j). Similar results regarding cell cycle distribution were obtained at 72 h of exposure, while further prolonging the incubation period increased cell death and reduced the number of G0/G1-phase cells (Fig. 5a, b). The S-phase fraction was not different from vehicle-treated organoids at both time points (Fig. 5a, b). This suggests that topotecan differentially targeted G1/G0- and G2/M-phase cells. In addition, topotecan and the highest doses of melphalan showed similar cell cycle profiles (Fig. 5b), resulting in comparable killing effects in treated organoids (Fig. 5c, f, g, j).

Methotrexate induced S-phase arrest and subsequently prevented G2/M-phase entry (vs. vehicle, p = 0.0234 and p = 0.0465) (Fig. 5a, b). However, similar to 8 μM melphalan, the drug was not sufficient to substantially induce cell death at 24 h of exposure, consistent with $CC3^+$ staining (Fig. 5a–d, h, j). Prolonged exposure to

methotrexate simultaneously caused a reduction the number of G0/G1-phase cells and increased cell death in sub-G1-phase cells (vs. vehicle, $p < 0.0001$ and $p = 0.0031$) while maintaining action in S and G2/M phases (Fig. 5b). This indicated that methotrexate had a slow anticancer effect.

To increase efficiency in controlling tumor growth, combined melphalan and topotecan is used clinically[6], but the comparative genotoxic effect of combinatorial drugs, relative to each single drug, has been unknown. Hence, 16 µM melphalan and 11 µM topotecan were tested in tumor organoids. The combined drug regimen significantly reduced S-phase arrest relative to that induced by melphalan alone ($p < 0.0001$), in concert with increased cell death in sub-G1 phase ($p = 0.0105$) (Fig. 5a, b); this was consistent with an elevated number of $CC3^+$ cells ($p = 0.0329$) (Fig. 5e, g, i, j). Cell cycle distribution was generally similar to topotecan alone (Fig. 5b). The number of $CC3^+$ cells in treated organoids indicated that the combined drug regimen and topotecan alone had a comparable killing effect to that of 32 µM melphalan (Fig. 5j). Prolonged exposure to the combined drug regimen caused an increased G0/G1 fraction, relative to that induced by either agent alone, indicative of cell arrest (vs. melphalan, $p = 0.0053$) (Fig. 5b). This subsequently prevented S- and G2/M-phase entry in a significantly greater proportion of cells than melphalan alone ($p = 0.0007$ and $p = 0.0101$) (Fig. 5b). Altogether, this suggested that the genotoxic effect of the combined drug regimen was superior to melphalan alone; however, the combined drug regimen and topotecan alone appeared to have comparable effects in terms of cell cycle distribution and $CC3^+$ staining.

Combined treatment with melphalan and topotecan effectively targets neoplastic cone cells in organoids

Anticancer drugs had a genotoxic effect, as shown by elevated γ-H2AX foci in drug-treated organoids (Fig. S6); this ultimately caused cell death (Fig. 5c–i). Although the

combined drugs, topotecan and high-dose melphalan, equally induced cell death (Fig. 5j), viable tumor cells that might be capable of regrowth remained in organoids. We asked whether the remaining cells were proliferative tumor cones and which drugs showed rapid control (at 24 h of exposure) by preferentially destroying proliferative cells, rather than resting tumor cone cells. We labeled RXRγ, which is required for the proliferation and survival of RB[12]. Co-expression of RXRγ and Ki67 identified proliferative tumor cone cells and differentiated from RXRγ$^+$ Ki67$^-$ resting tumor cones (Fig. 6a–u). RXRγ staining indicated that cuboidal or column-shaped cells were maintained as in-vehicle-organoids, suggestive of low efficacy of low and medium doses of melphalan and methotrexate (Fig. 6a, d, g, p). In contrast, organoid cells were transformed into round shapes with the high doses of melphalan, topotecan, and the combined drug regimen (Fig. 6j, m, s). Vehicle-treated organoids consisted of 83.3 ± 2.2% of RXRγ$^+$ cells and 69.2 ± 5.7% of RXRγ$^+$ Ki67$^+$ cells; thus, the cell ratio of RXRγ$^+$ Ki67$^+$ to RXRγ$^+$ was 83.0 ± 5.4% (mean ± SEM) (Fig. 6a–c, v). We found that at 24 h exposure, proportions of viable RXRγ$^+$ cells in drug-treated organoids remained as in-vehicle-organoids (Fig. 6a–v). Topotecan and the combined drug regimen both significantly reduced the proportions of viable RXRγ$^+$ Ki67$^+$ cells (23.5 ± 7.6%, p = 0.0130; 20 ± 4.6%, p = 0.0076) and cell ratios of RXRγ$^+$ Ki67$^+$ to RXRγ $^+$ (48.7 ± 2.0%, p = 0.0046; 36.6 ± 3.1%, p = 0.0003) (Fig. 6m–o and s–v). This suggested that topotecan, both alone and in combination with melphalan, targeted proliferative tumor cones. In comparison with topotecan alone, the combined drug regimen demonstrated an enhanced effect in reducing proliferative tumor cones (the highest single agent model: CI = 0.74) (Fig. 6w).

Discussion

Culture systems greatly impact the maintenance of tumorigenic aspects in primary tumor-derived cells. Two-dimensional adherent cultures, despite being amenable to high-throughput screening, do not recapitulate and rarely represent clinically relevant patient tissues[33]. The advent of organoid cultures has allowed recapitulation of 3-D, self-organizing cellular structures that resemble tissue. Here, we demonstrated that tumor organoids can be derived from a tumor of the retina and can retain molecular and cellular features of the parental tumor. Additionally, as a model of vitreous seeds tumor organoids produced different drug responses that can be used to predict anticancer drug activities for seed control.

Two subgroups of RB with biallelic loss of the *RB1* gene have been identified; both exhibit gene expression signatures of cone photoreceptors, although the cone-associated genes are expressed more highly in one group than the other[34]. The reduced expression of cone-associated genes is proposed to associate with increased genomic alterations, which contribute to tumor progression[35]. Consistently, RB organoids in our study exhibited well-preserved cone gene expression signatures and cone-specific proteins, reflective of the tumor cell of origin. In addition, irregular expression of genes associated with mesodermal cell lineage in tumor cells with cone signatures reflects intrinsic properties of RB that possess invasive and metastatic capacities; this indicates that organoids are well-represented vitreous seeds. We detected additional regional gains in organoids, which could represent undetectable genomic disruptions within the original tumors and may coevolve through a Darwinian selection process to increase the fitness of the overall tumor population[36]. These alterations, such as regional 2p gain, have been documented in primary RB[31, 32] and allow the emergence of a complex clonal architecture that may underlie tumor proliferation, progression, or drug resistance.

Analysis of RB1-depleted retinal cells identifies differentiating cones as tumor-initiating cells that form RB-like tumors in orthotopic xenografts[13]. Human cone-specific signaling circuitry sensitizes to cancerous transformation and collaborates with RB1 depletion[12, 13]. An intrinsically high level of expression of the MDM2 proto-oncogene in human cones predisposes them to transformation by preventing cell death[12, 37]. MDM2 expression is regulated by the cone-specific RXRγ, which, together with TRβ2, is required for the proliferation and survival of RB[12, 38]. The expression of MDM2 is not detected in xenografts[7], but was expressed in our tumor organoids, together with RXRγ and TRβ2. This indicates that organoids retain cone-specific signaling circuitry, suggesting the use of tumor organoids as a model for examining targeted therapies specifically designed to destroy this circuitry.

Organoids provide opportunities for testing the accessibility of therapeutic agents and ex vivo screening of drug sensitivities. We found that combined treatment with topotecan and melphalan was more effective than melphalan alone, consistent with clinical outcomes observed in attempts to control vitreous seeds[6]. Melphalan (20–30 µg) is extensively used in intravitreal chemotherapy, but in some cases fails to control recurrent and refractory seeds[1, 3]. The combined drug regimen achieves rapid control of seeds, such that fewer cycles of chemotherapy are required, compared with melphalan alone [6]. Because of its limited toxicity[39], topotecan alone has been recently used to manage persistent vitreous seeds with satisfactory outcomes; its efficacy is between that of melphalan alone and the combined drug regimen[4], consistent with our results. Partial control of seeds has been achieved with low-dose melphalan (8–10 µg), consistent with our results. Higher doses of melphalan (>40 µg) cause ocular complications[2]. Unlike other drugs, methotrexate showed slow effects

and exhibited the lowest efficacy, consistent with the need for multiple injections over a longer period of treatment[5]. Organoids showed that topotecan alone and in combination with melphalan effectively targeted proliferative cones, rather than non-proliferative cones. Topotecan, a topoisomerase I inhibitor, induces rapid cellular stress in G1, G2, and S phases, thereby causing failure to engage mitosis[40], which is consistent with our results. We routinely used melphalan and methotrexate with variable success in controlling vitreous seeds. The results of the current study are consistent with previous reports[4, 6] that encouraged the use of topotecan and melphalan in management of vitreous seeds.

The tumor microenvironment, or tumor stroma, is highly responsible for growth, metastasis, and drug resistance through paracrine effects[41, 42]. Glial cells with astrocyte properties, which serve as the tumor microenvironment, promote proliferation and survival of RB[43]. Organoids and tumor tissue contained glial cells, as indicated by $GFAP^+$ cell staining, which constitute ~2–3% of the cells in RB tumors[12]. The expression of GDNF (by glia or fibroblasts), and its cognate receptor RET, in organoids and the parental tumor (Fig. S5b, c) implies crosstalk between RB glia and tumor cells. Unlike tumor organoids, $GFAP^+$ cells are absent in tumorspheres derived from RB[33], representing a clear advantage of organoids in generating a close-to-patient model.

In the era of precision medicine, faithful preclinical models are important for guiding treatment options. Organoid technology offers simple and efficient generation of 3-D-tumor tissue models. RB organoid models retained cone signal circuitry and produced clinically relevant drug responses, thus facilitate development of targeted

444 therapies that can be used in management of vitreous seeds. As a model, organoids
445 could accelerate the discovery of novel therapies, while reducing animal usage and
446 costs invested in therapeutic development.

447

448 **Materials and Methods**

449 **Human tissues**

450 RB tissues (stage E, according to the International Classification for Intraocular RB)
451 were collected directly from patients undergoing enucleation. Tumor tissue samples
452 after incision were used for organoid culture and for analyses of DNA copy number
453 alterations and gene expression profiles. Blood was drawn from patients for analysis
454 of DNA copy number. All experimental protocols were approved by IRB at Faculty of
455 Medicine, Ramathibodi Hospital, Mahidol University (protocol number ID11-58-53
456 and ID07-60-14). All methods were performed in accordance with the relevant
457 guidelines and regulations. Informed consent was obtained from a parent of patients
458 before collecting the samples.

459 **RB organoid culture**

460 Primary RB samples were collected in ice-cold Dulbecco's Modified Eagle Medium:
461 Nutrient Mixture F-12 (DMEM/F-12) containing antibiotics. Tumor tissues were finely
462 minced and incubated in ACCUMAX™ (Chemicon) for 30 min at 37°C. One volume
463 of PBS was added to the cell solution, which was then centrifuged at 300 × *g* for 5
464 min. Supernatant was removed and cell pellets were resuspended in cold organoid
465 medium (Neurobasal medium (Invitrogen) supplemented with 20 ng/mL epidermal
466 growth factor (EGF; R&D Systems), 10 ng/mL basic fibroblast growth factor (bFGF;
467 Peprotech), 1X B27 (Invitrogen), 2.5% knockout serum replacement (KSR), 2.5%

fetal bovine serum (FBS), 20 mM Glutamax, 1 mM sodium pyruvate, 0.25 µg/mL amphotericin B, and 100 U/mL penicillin-streptomycin. Tumor cell solution was embedded in Matrigel® (growth factor reduced, Corning) at a 1:1.8 ratio of cell solution to Matrigel® solution. A total of 20 µL mixed cell-gel solution was added to six-well plates via 5-7 drops/well and solidified in an incubator (37°C) for 30–45 min. Organoid medium was added to cover the gel drops and cultures were maintained in a humidified incubator, with 5% CO_2, at 37°C. RB organoids were manually dissociated and passaged at a 1:3 or 1:4 ratio every 3–4 weeks by embedding in fresh Matrigel®. Cold freezing medium (organoid medium containing 10% dimethylsulfoxide) was used to freeze organoids at -80°C for 24 h prior to long-term storage in liquid nitrogen.

Drug treatments

Drugs (pharmaceutical grade) were further diluted with 0.9% NaCl to obtain concentrations equivalent to the final clinical dose achieved in the vitreous, including melphalan at 8 (10), 16 (20) and 32 (40) µM (µg of delivered drugs in vitreous-containing 4 mL fluid), methotrexate at 275 µM (400 µg), and a combination of melphalan at 16 µM (20 µg) and topotecan at 11 µM (30 µg). Organoids (< passage 5) were incubated with drugs for 24 or 72 h. NaCl (0.02% final concentration in culture) was used as a control.

Histology, immunofluorescence and imaging, cell cycle, copy number, and gene expression analyses are described in the Supplementary information.

Data Availability

All data generated or analyzed during this study are included in this published article and its Supplementary Information files.

References

1. Berry, J.L. *et al*. Not all seeds are created equal: seed classification is predictive of outcomes in RB. *Ophthalmology*. **124**, 1817–1825 (2017).
2. Ghassemi, F. & Shields, C.L. Intravitreal melphalan for refractory or recurrent vitreous seeding from retinoblastoma. *Arch Ophthalmol*. **130**, 1268–1271 (2012).
3. Shields, C.L. *et al*. Intravitreal melphalan for persistent or recurrent retinoblastoma vitreous seeds: preliminary results. *JAMA Ophthalmol*. **132**, 319–325 (2014).
4. Rao, R., Honavar, S.G., Sharma, V. & Reddy, VAP. Intravitreal topotecan in the management of refractory and recurrent vitreous seeds in retinoblastoma. *Br J Ophthalmol*. **102**, 490–495 (2017).
5. Kivelä, T., Eskelin, S. & Paloheimo, M. Intravitreal methotrexate for retinoblastoma. *Ophthalmology*. **118**, 1689–1689.e6 (2011)
6. Ghassemi, F., Shield,s C.L., Ghadimi, H., Khodabandeh, A. & Roohipoor, R. Combined intravitreal melphalan and topotecan for refractory or recurrent vitreous seeding from retinoblastoma. *JAMA Ophthalmol*. **132**, 936–941 (2014).
7. McEvoy, J. *et al*. Coexpression of normally incompatible developmental pathways in retinoblastoma genesis. *Cancer Cell*. **20**, 260–275 (2011).
8. Nair, RM. & Vemuganti, GK. Transgenic models in retinoblastoma research. *Ocul Oncol Pathol*. **1**, 207–213 (2015).
9. MacPherson, D. *et al*. Cell type-specific effects of Rb deletion in the murine retina. *Genes Dev*. **18**, 1681–1694 (2004).

10. Chen, D. *et al*. Cell-specific effects of RB or RB/p107 loss on retinal development implicate an intrinsically death-resistant cell-of-origin in retinoblastoma. *Cancer Cell*. **5**, 539– 551 (2004).

11. Aldiri, I. *et al*. The dynamic epigenetic landscape of the retina during development, reprogramming, and tumorigenesis. *Neuron.* **94**, 550–568.e10 (2017).

12. Xu, X.L.*et al*. Retinoblastoma has properties of a cone precursor tumor and depends upon cone-specific MDM2 signaling. *Cell*. **137**, 1018–3101 (2009).

13. Xu, X.L.*et al*. Rb suppresses human cone-precursor-derived retinoblastoma tumours. *Nature.* **514**, 385–388 (2014).

14. Benavente, C.A. *et al*. Cross- species genomic and epigenomic landscape of retinoblastoma. *Oncotarget*. **4**, 844–859 (2013).

15. Zhang, J. *et al*. A novel retinoblastoma therapy from genomic and epigenetic analyses. *Nature*. **481**, 329–334 (2012).

16. Dutta, D., Heo, I. & Clevers, H. Disease modeling in stem cell-derived 3D organoid systems. *Trends Mol Med*. **23**, 393–410 (2017).

17. Fatehullah, A., Tan, S.H. & Barker, N. Organoids as an in vitro model of human development and disease. *Nat Cell Biol*. **18**, 246–254 (2016).

18. Hoshino, A. *et al*. Molecular Anatomy of the Developing Human Retina. *Dev Cell*. **18**, 763–779.e4 (2017).

19. Kaewkhaw, R. *et al*. Transcriptome dynamics of developing photoreceptors in three-dimensional retina cultures recapitulates temporal sequence of human cone and rod differentiation revealing cell surface markers and gene networks. *Stem Cells.* **33**, 3504–3518 (2015).

20. Kaewkhaw R. *et al*. Treatment paradigms for retinal and macular diseases using 3-D retina cultures derived from human reporter pluripotent stem cell lines. *Invest Ophthalmol Vis Sci*. **57**, ORSFl1–ORSFl11 (2016).

21. Fujii, M. *et al*. A colorectal tumor organoid library demonstrates progressive loss of niche factor requirements during tumorigenesis. *Cell Stem Cell*. **18**, 827–838. (2016).

22. van de Wetering, M. *et al*. Prospective derivation of a living organoid biobank of colorectal cancer patients. *Cell*. **161**, 933–945 (2015).

23. Sachs, N. *et al*. A living biobank of breast cancer organoids captures disease heterogeneity. *Cell*. **172**, 373–386.e10 (2018).

24. Broutier, L. *et al*. Human primary liver cancer-derived organoid cultures for disease modeling and drug screening. *Nat Med*. **23**, 1424–1435 (2017).

25. Gao, D. *et al*. Organoid cultures derived from patients with advanced prostate cancer. *Cell*. **159**, 176–187 (2014).

26. Baker, L.A., Tiriac, H., Clevers, H. & Tuveson, D.A. Modeling pancreatic cancer with organoids. *Trends Cancer*. **2**, 176–190 (2016).

27. Traverso, V., Kinkl, N., Grimm, L., Sahel, J. & Hicks, D. Basic fibroblast and epidermal growth factors stimulate survival in adult porcine photoreceptor cell cultures. *Invest Ophthalmol Vis Sci.* **44**, 4550–4558 (2003).

28. Roberts, M.R., Hendrickson, A., McGuire, C.R. & Reh, T.A. Retinoid X receptor γ is necessary to establish the S-opsin gradient in cone photoreceptors of the developing mouse retina. *Invest Ophthalmol Vis Sci*. **46**, 2897–2904 (2005).

29. Ng, L. *et al.* Two transcription factors can direct three photoreceptor outcomes from rod precursor cells in mouse retinal development. *J Neurosci.* **31**, 11118–11125 (2011).

30. Corson, T.W. & Gallie, B.L. One hit, two hits, three hits, more? Genomic changes in the development of retinoblastoma. *Genes Chromosomes Cancer*. **46**, 617–634 (2007).

31. McEvoy, J. *et al*. RB1 gene inactivation by chromothripsis in human retinoblastoma. *Oncotarget*. **5**, 438–450 (2014).

32. Kooi, I.E.*et al.* A meta-analysis of retinoblastoma copy numbers refines the list of possible driver genes involved in tumor progression. *PLoS One*. **11**, e0153323 (2016).

33. Bond, W.S. *et al.* Tumorspheres but not adherent cells derived from retinoblastoma tumors are of malignant origin. *PLoS One.* **8**, e63519 (2013).

34. Kapatai, G. *et al*. Gene expression profiling identifies different sub-types of retinoblastoma. *Br J Cancer*. **109**, 512–525 (2013).

35. Kooi, I.E. *et al*. Loss of photoreceptorness and gain of genomic alterations in retinoblastoma reveal tumor progression. *EBioMedicine*. **2**, 660–670 (2015).

36. Burrell, R.A., McGranahan, N., Bartek, J. & Swanton, C. The causes and consequences of genetic heterogeneity in cancer evolution. *Nature*.**501**, 338–345 (2013).

37. Qi, D-L. & Cobrinik, D. MDM2 but not MDM4 promotes retinoblastoma cell proliferation through p53-independent regulation of MYCN translation. *Oncogene.* **36**, 1760–1769 (2017).

38. Xu, X.L. *et al*. SKP2 activation by thyroid hormone receptor β2 bypasses Rb-dependent proliferation in Rb-deficient cells. *Cancer Research*. **77**, 6838–6850 (2017).

39. Buitrago, E. *et al*. Ocular and systemic toxicity of intravitreal topotecan in rabbits for potential treatment of retinoblastoma. *Exp Eye Res*. **108**, 103–109 (2013).

40. Feeney, G.P. *et al*. Tracking the cell cycle origins for escape from topotecan action by breast cancer cells. *Br J Cancer*. **88**, 1310–1317 (2003).

41. Onion, D. *et al*. 3-dimensional patient-derived lung cancer assays reveal resistance to standards-of-care promoted by stromal cells but sensitivity to histone deacetylase inhibitors. *Mol Cancer Ther.* **15**, 753–763 (2016).

42. Bremnes, R.M. *et al*. The role of tumor stroma in cancer progression and prognosis: emphasis on carcinoma-associated fibroblasts and non-small cell lung cancer. *J Thorac Oncol*. **6**, 209–217 (2011).

43. Xu, X.L. *et al*. Tumor-associated retinal astrocytes promote retinoblastoma cell proliferation through production of IGFBP-5. *Am J Pathol*. **177**, 424–435 (2010).

Acknowledgments

We thank Koset Pinpradap, Histopathology Core Facility, Ramathibodi Hospital, for technical support in tissue processing for hematoxylin and eosin staining. We also thank Anand Swaroop (N-NRL, National Eye Institute, NIH) for helpful comments and discussion and Ryan Chastain-Gross, Ph.D., from Edanz Group (www.edanzediting.com/ac) for editing a draft of this manuscript. This work was funded by the Thailand Research Fund and Commission on Higher Education (CHE) (MRG 5980031), Mahidol University, Talent Management Grant and Faculty of Medicine Ramathibodi Hospital (RF_59030 and CF_60002) to RK. CF_60002 was also granted to DR.

Authors' Contributions

Conception and design: DS, DR, SH and RK

Development of methodology: DS, PC, TB, WT and RK

Acquisition of data: DS, PC, TB, WT, and RK

Analysis and interpretation of data: DS, VC, NJ and RK

Writing, review, and/or revision of the manuscript: VC, SH and RK

Technical or material support: DR, RA and NJ

Study supervision: SH and RK

Competing Interests: The authors declare no competing interests.

Figure Legends

Figure 1. Establishment of retinoblastoma organoid cultures

(**a**) Photograph of retinoblastoma organoids grown in Matrigel® drops. (**b**) Mosaic image shows of multiple organoid sizes in a single Matrigel® drop; typical growth features of a 3-week culture after passaging. (**c**) Magnified micrograph of organoids showing dense cellular organization. (**d–f**) Confocal z-plane images of whole-mount organoid (bottom to top), stained with phalloidin and 4',6-diamidino-2-phenylindole (DAPI), showing multiple rosette formation (dashed-line circles indicate inserted images). Scale bar, 1 cm (a); 1000 µm (b); 200 µm (c) and 100 µm (d–f).

Figure 2. Reproducible cellular features and contents of the retinoblastoma in tumor organoids

(**a–c**) Hematoxylin and eosin staining of the enucleated globe (a). Arrows in (a) indicate magnified regions showing choroid (b) and optic nerve (c, (arrow)) invasion. (**d–g**) Representative micrographs indicate histological features of parental tumor tissue (d, e) and organoids (f, g). Dashed-line squares in (d, e) indicate magnified regions presented in (f, g). Flexner-Wintersteiner (arrowhead) and Homer-Wright (arrow) rosettes (f, g) were maintained in organoids. (**h–o**), Representative micrographs of immunostaining indicate the expression of Ki67 and cone-specific proteins [RXRγ (h, i), TRβ2 (staining specificity demonstrated by Xu et al.[12]) (j, k), M/L opsin (l, m)] or glial fibrillary acidic protein [GFAP (n, o)] in parental tumor tissue and organoids. Nuclei stained by 4',6-diamidino-2-phenylindole (DAPI). Scale bar, 5 mm (a); 200 µm (b, c); 100 µm (d, e) and 50 µm (f–o). See Fig. S2 for other retinal markers.

Figure 3. DNA copy number landscape of patient-derived retinoblastoma organoid line

(**a, b**) Copy number aberration of regional gains and losses (>3 Mb) (a) and focal lesions (<3 Mb) (b) in retinoblastoma (RB) tissue, organoids (O) at passage 1 (P1, 6-week culture), 3 (P3, 13-week culture), and 5 (P5, 19-week culture), matched with peripheral blood. See Fig. S3 for the frequency of gains or losses in tissue and organoids.

Figure 4. Tumor organoids recapitulate gene expression profile of primary retinoblastoma tissue of origin

(**a**) Correlation heat map between organoids (O) at passage 1 (P1, 6-week culture) and 3 (P3, 13-week culture), the corresponding patient-derived retinoblastoma (RB) and published transcriptomes of retinoblastoma (RB^{*}) and fetal retina (FR^{1} and FR^{2}). (**b, c**) heat maps show differentially expressed genes of the two most significant gene ontologies (GOs), associated with sensory perception (b) and cell fate commitment (c). See Fig. S5 for other GOs and their corresponding gene expression profiles.

Figure 5. Chemotherapeutic drug responses of tumor organoids

(**a, b**) Cell cycle analysis of organoids in response to anticancer drugs at 24 (a, b) and 72 (b) h after drug administration. Statistical analysis of cell cycle phases at each time point (mean percentage ± SEM, n=3) was conducted by one-way ANOVA followed by Tukey's test. (**c–i**) Representative micrographs of immunostaining for cleaved caspase 3 (CC3), an indicative marker of apoptotic cells in organoids treated

with vehicle (c), 8 (d), 16 (e), or 32 (f) µM melphalan (Mel), 11 µM topotecan (Topo) (g), 275 µM methotrexate (Metho) (h), or the combined regimen of 16 µM melphalan with 11 µM topotecan (i). Nuclei stained by 4',6-diamidino-2-phenylindole (DAPI). Scale bar, 50 µm. (**j**) Bar graph indicates % $CC3^+$ cells (mean percentage ± SEM, n=3) after exposure to drugs for 24 h. Mean percentages were determined from 7–10 micrographs containing 300–500 cells for each condition. Statistical analysis of % $CC3^+$ cells was conducted by one-way ANOVA followed by Tukey's test. The p values of single or combined agents vs. vehicle for cell cycle analysis are listed in the text.

Figure 6. Cone cell features in organoids in response to anticancer drugs at 24 h.

(**a–u**) Representative micrographs of immunostaining for cone marker RXRγ (a, d, g, j, m, p, and s) and proliferative marker Ki67 (b, e, h, k, n, q, and t) in organoids treated with vehicle (a–c), 8 (d–f), 16 (g–i), or 32 (j–l) µM melphalan (Mel), 11 µM topotecan (Topo) (m–o), 275 µM methotrexate (Metho) (p–r), or the combined regimen of 16 µM melphalan with 11 µM topotecan (s–u). Merged images (c, f, i, l, o, r, and u). Nuclei stained by 4',6-diamidino-2-phenylindole (DAPI). Scale bar, 50 µm. (**v**) Bar graph shows % $RXR\gamma^+$ cells (non-proliferative cones), $RXR\gamma^+$ cells co-stained with Ki67 (proliferative cones), and ratio of proliferative to non-proliferative cones (mean percentages ± SEM, n=3). Mean percentages (proportions) were determined in nine micrographs for each condition. Statistical analysis of % positive cells was conducted by one-way ANOVA followed by Dunnett's test. (**w**) Bar graph shows death of cell ratio of $RXR\gamma^+$ $Ki67^+$ to $RXR\gamma^+$ (mean percentages ± SEM, n=3, unpaired t-test).

718

719 **Figure 1**

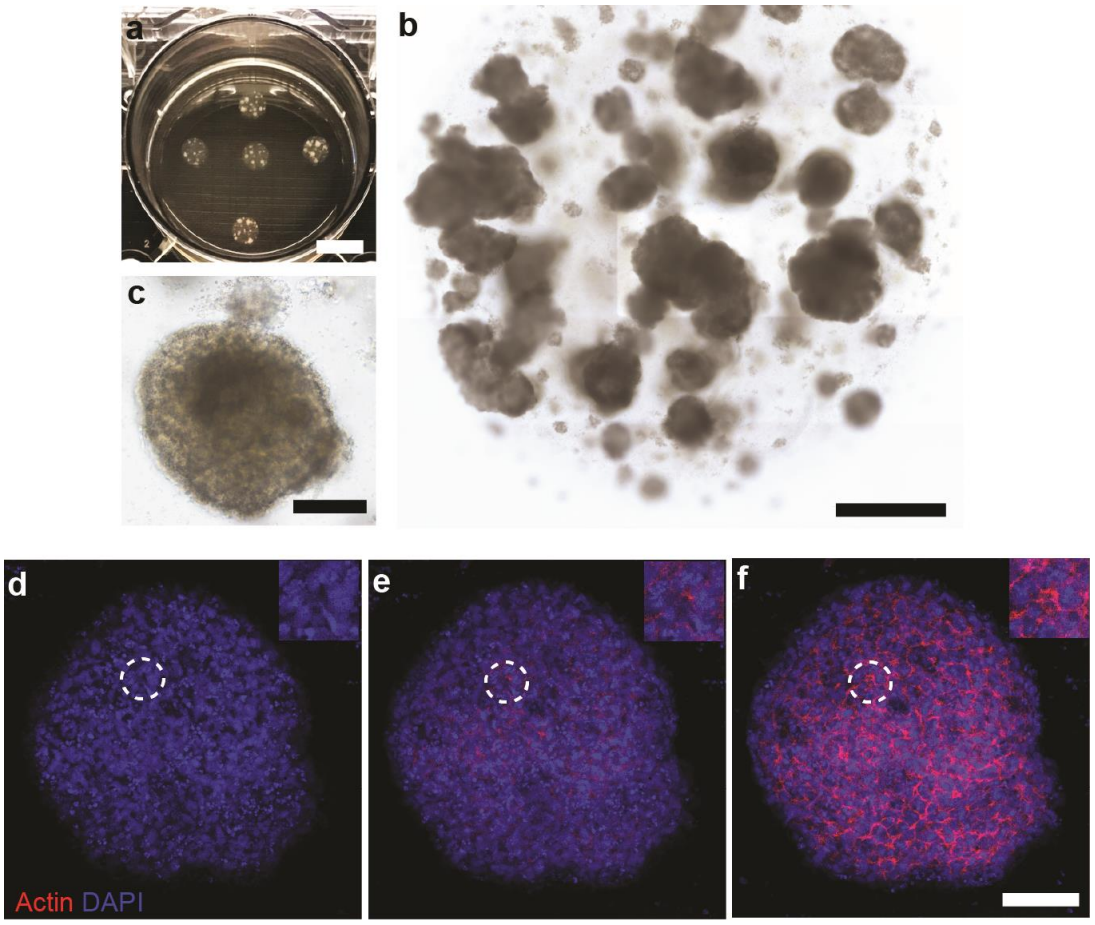

720

721

722

723

724

725

726

727

728

Figure 2

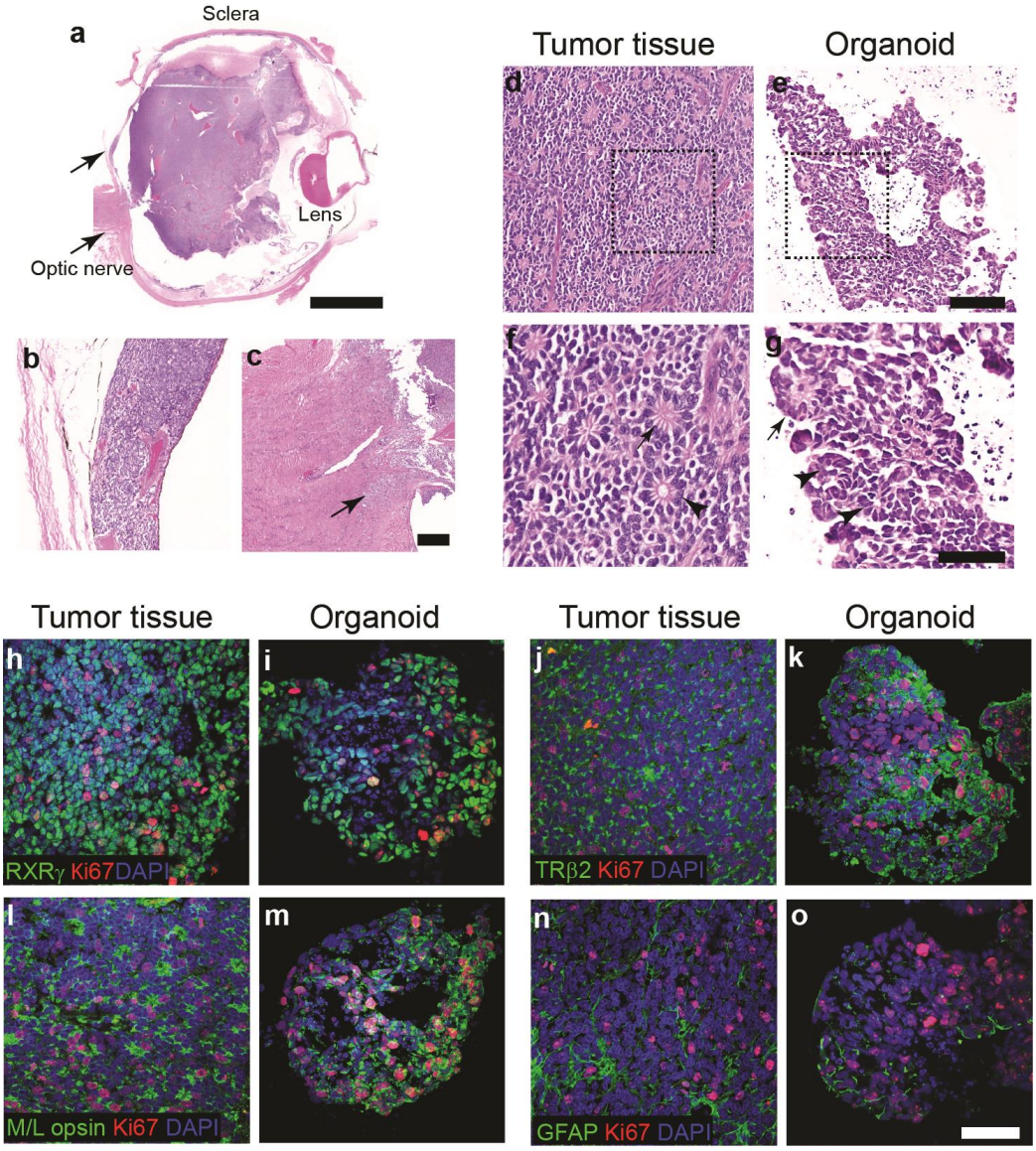
a
Sclera
Lens
Optic nerve
b
c
Tumor tissue
Organoid
d
e
f
g
Tumor tissue
Organoid
Tumor tissue
Organoid
h
i
j
k
RXRγ Ki67DAPI
TRβ2 Ki67 DAPI
l
m
n
o
M/L opsin Ki67 DAPI
GFAP Ki67 DAPI

Figure 3

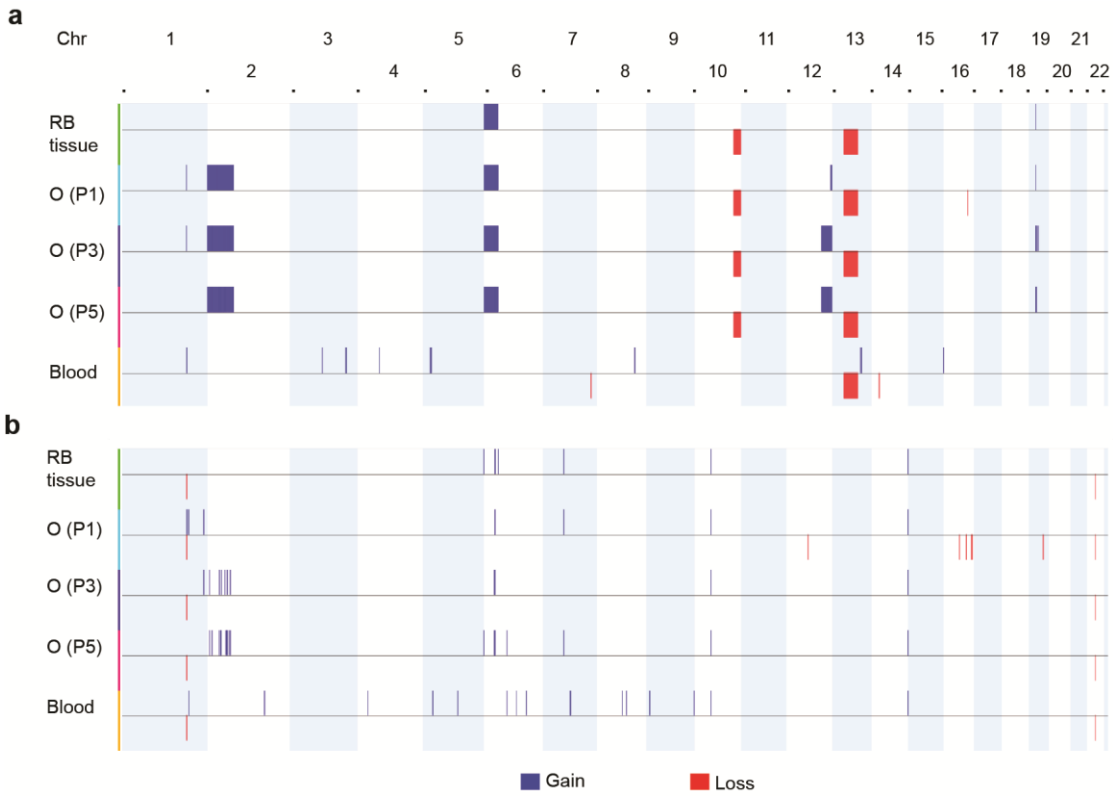
a
Chr
1
2
3
4
5
6
7
8
9
10
11
12
13
14
15
16
17
18
19
20
21
22
RB tissue
O (P1)
O (P3)
O (P5)
Blood
b
RB tissue
O (P1)
O (P3)
O (P5)
Blood
Gain
Loss

Figure 4

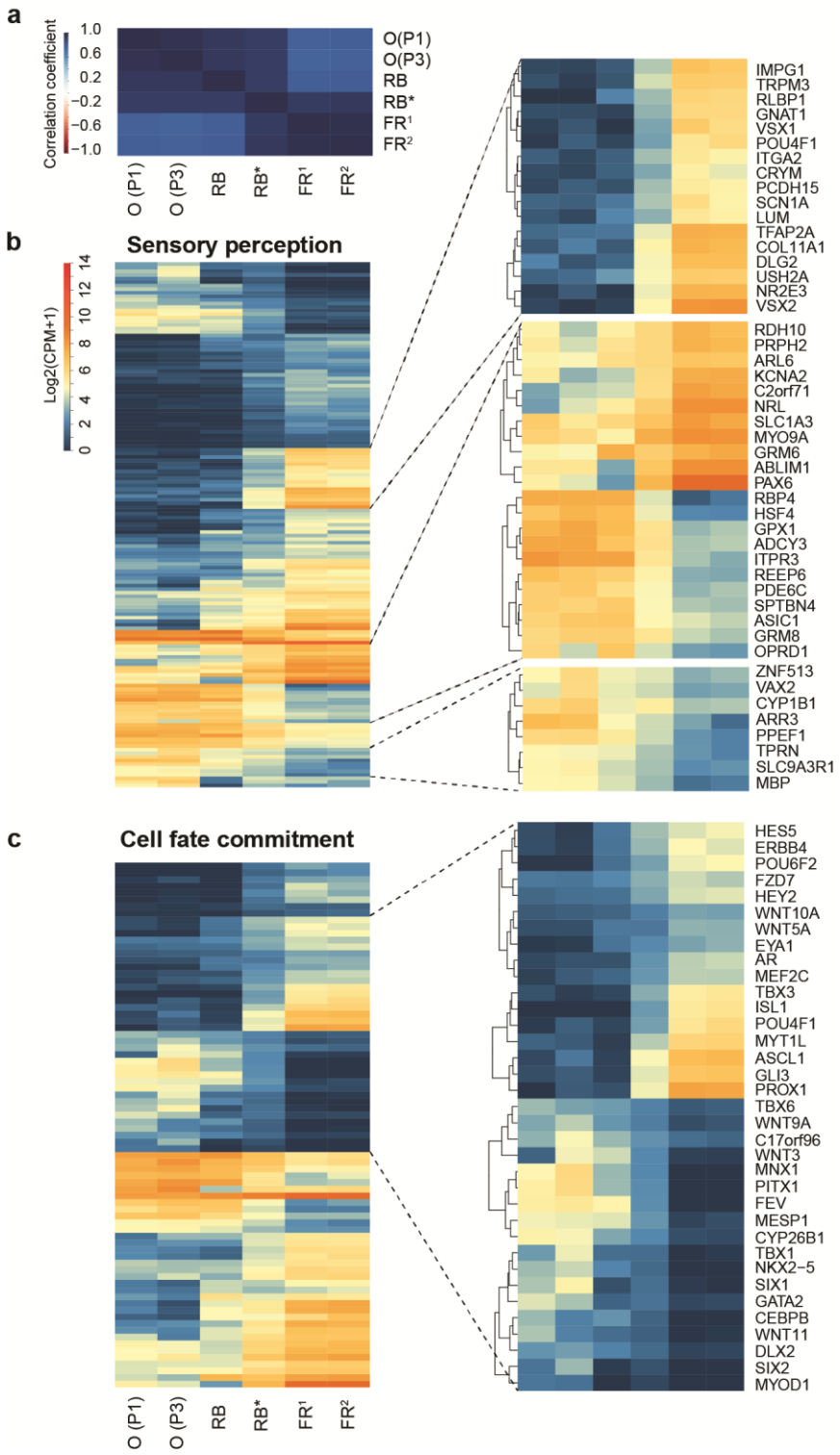
a
Correlation coefficient
1.0
0.6
0.2
−0.2
−0.6
−1.0
O(P1)
O(P3)
RB
RB*
FR¹
FR²
O (P1)
O (P3)
RB
RB*
FR¹
FR²
b
Sensory perception
Log2(CPM+1)
0 2 4 6 8 10 12 14
IMPG1
TRPM3
RLBP1
GNAT1
VSX1
POU4F1
ITGA2
CRYM
PCDH15
SCN1A
LUM
TFAP2A
COL11A1
DLG2
USH2A
NR2E3
VSX2
RDH10
PRPH2
ARL6
KCNA2
C2orf71
NRL
SLC1A3
MYO9A
GRM6
ABLIM1
PAX6
RBP4
HSF4
GPX1
ADCY3
ITPR3
REEP6
PDE6C
SPTBN4
ASIC1
GRM8
OPRD1
ZNF513
VAX2
CYP1B1
ARR3
PPEF1
TPRN
SLC9A3R1
MBP
c
Cell fate commitment
HES5
ERBB4
POU6F2
FZD7
HEY2
WNT10A
WNT5A
EYA1
AR
MEF2C
TBX3
ISL1
POU4F1
MYT1L
ASCL1
GLI3
PROX1
TBX6
WNT9A
C17orf96
WNT3
MNX1
PITX1
FEV
MESP1
CYP26B1
TBX1
NKX2−5
SIX1
GATA2
CEBPB
WNT11
DLX2
SIX2
MYOD1
O (P1)
O (P3)
RB
RB*
FR¹
FR²

Figure 5

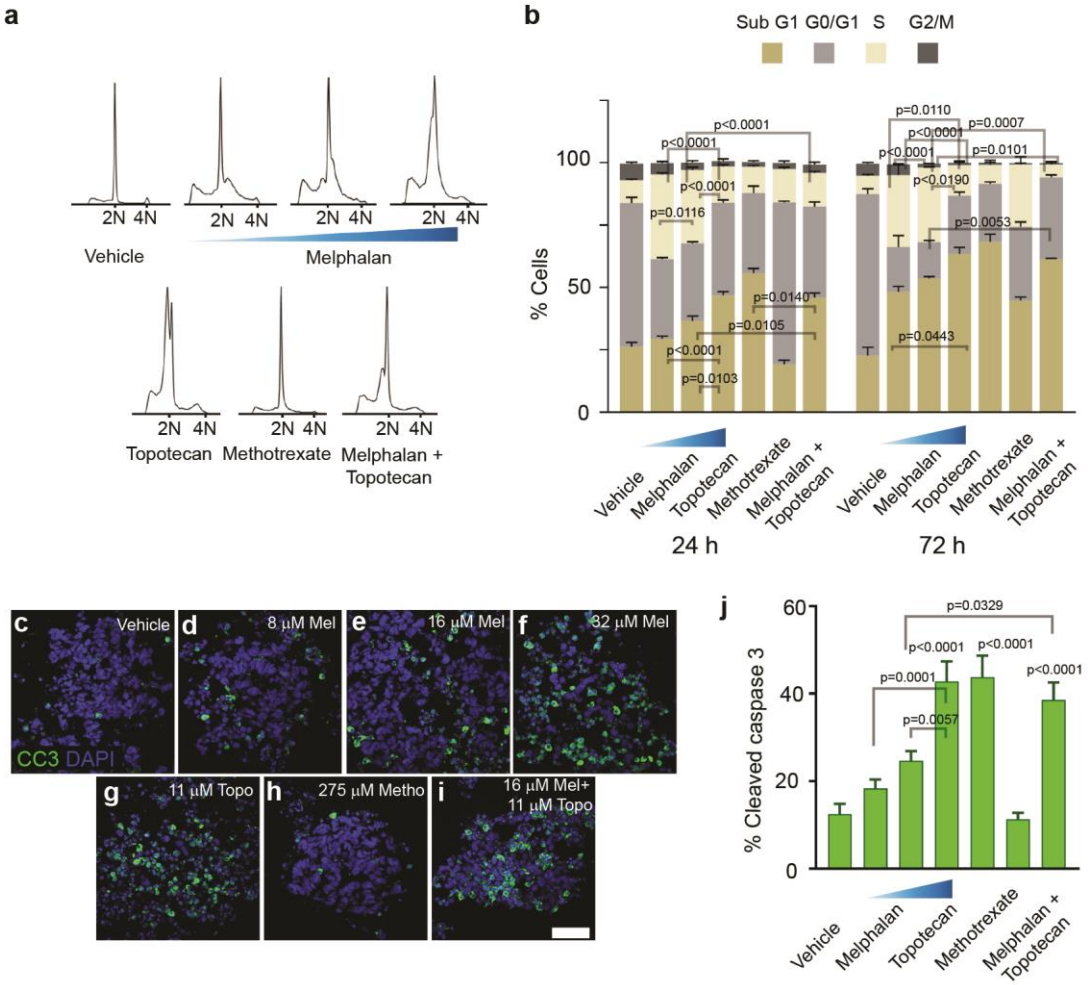
a
2N 4N
Vehicle
Melphalan
Topotecan
Methotrexate
Melphalan + Topotecan
b
Sub G1 G0/G1 S G2/M
% Cells
24 h
72 h
Vehicle
Melphalan
Topotecan
Methotrexate
Melphalan + Topotecan
c Vehicle
d 8 μM Mel
e 16 μM Mel
f 32 μM Mel
CC3 DAPI
g 11 μM Topo
h 275 μM Metho
i 16 μM Mel+ 11 μM Topo
j
% Cleaved caspase 3

Figure 6

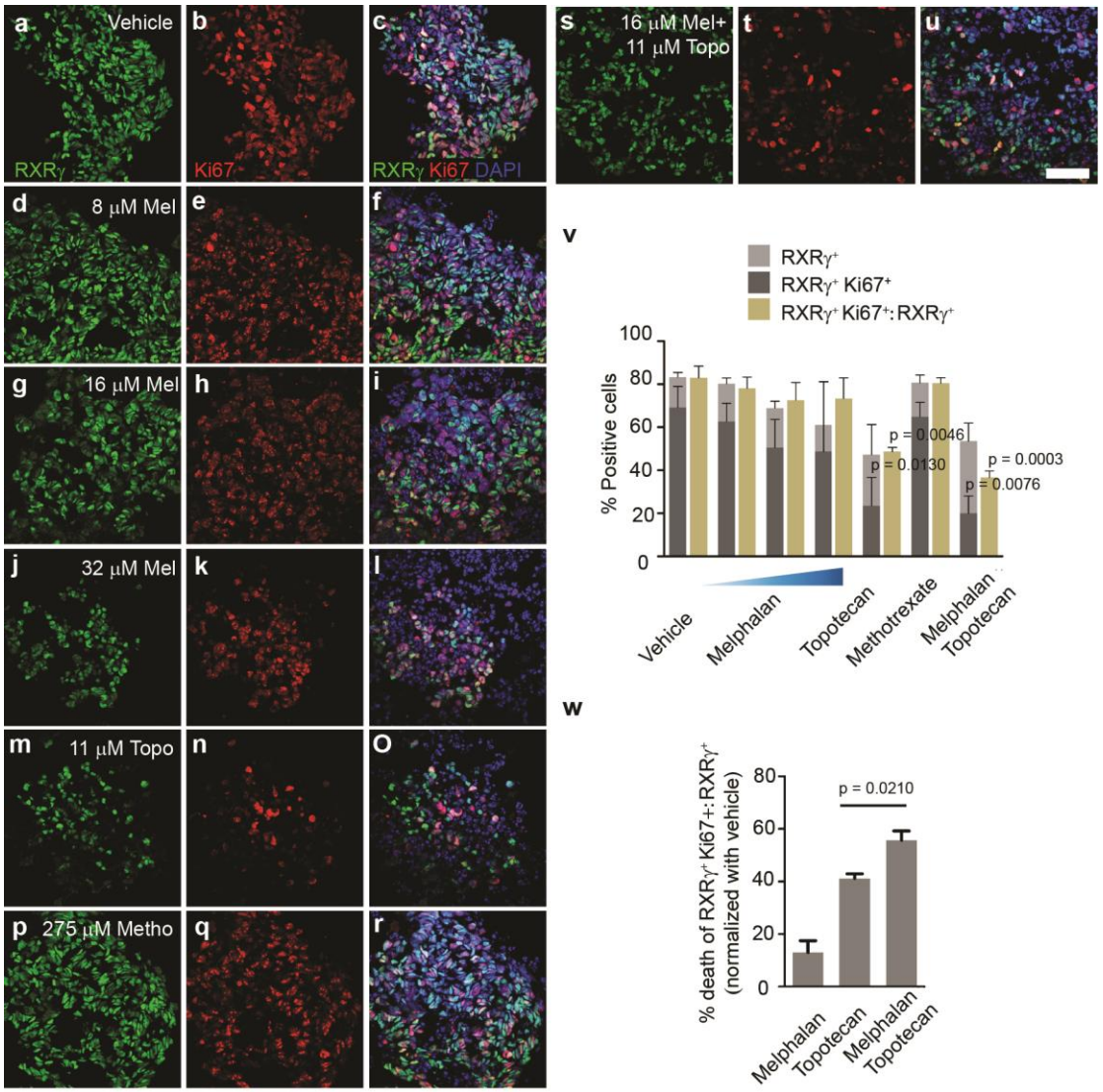
a Vehicle
RXRγ
b
Ki67
c
RXRγ Ki67 DAPI
d 8 μM Mel
e
f
g 16 μM Mel
h
i
j 32 μM Mel
k
l
m 11 μM Topo
n
O
p 275 μM Metho
q
r
s 16 μM Mel+
11 μM Topo
t
u
v
RXRγ+
RXRγ+ Ki67+
RXRγ+ Ki67+:RXRγ+
% Positive cells
100
80
60
40
20
0
p = 0.0046
p = 0.0130
p = 0.0003
p = 0.0076
Vehicle
Melphalan
Topotecan
Methotrexate
Melphalan
Topotecan
w
% death of RXRγ+ Ki67+:RXRγ+
(normalized with vehicle)
80
60
40
20
0
p = 0.0210
Melphalan
Topotecan
Melphalan
Topotecan